ISSN 2096-7071 (Print)
ISSN 2096-3101 (Online)
CN 10-1629/R1

CHINA CDC WEEKLY

CCDC weekly
Vol. 6 No. 20 May 17, 2024
中国疾病预防控制中心周报

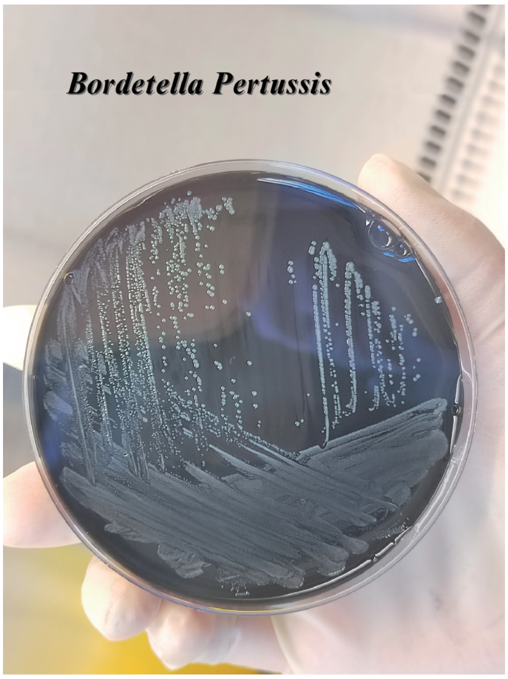

INFECTIOUS DISEASE ISSUE

Preplanned Studies

Vital Surveillances

Methods and Applications

ISSN 2096-7071
9 772096 707248 20

Editorial Board

Editor-in-Chief Hongbing Shen
Founding Editor George F. Gao
Deputy Editor-in-Chief Liming Li Gabriel M Leung Zijian Feng
Executive Editor Chihong Zhao

Members of the Editorial Board

Rui Chen
Wen Chen
Xi Chen (USA)
Zhuo Chen (USA)
Gangqiang Ding
Xiaoping Dong
Pei Gao
Mengjie Han
Yuantao Hao
Na He
Yuping He
Guoqing Hu
Zhibin Hu
Yueqin Huang
Na Jia
Weihua Jia
Zhongwei Jia
Guangfu Jin
Xi Jin
Biao Kan
Haidong Kan
Ni Li
Qun Li
Ying Li
Zhenjun Li
Min Liu
Qiyong Liu
Xiangfeng Lu
Jun Lyu
Huilai Ma
Jiaqi Ma
Chen Mao
Xiaoping Miao
Ron Moolenaar (USA)
Daxin Ni
An Pan
Lance Rodewald (USA)
William W. Schluter (USA)
Yiming Shao
Xiaoming Shi
Yuelong Shu
RJ Simonds (USA)
Xuemei Su
Chengye Sun
Quanfu Sun
Xin Sun
Feng Tan
Jinling Tang
Huaqing Wang
Hui Wang
Linhong Wang
Tong Wang
Guizhen Wu
Jing Wu
Xifeng Wu (USA)
Yongning Wu
Min Xia
Ningshao Xia
Yankai Xia
Lin Xiao
Wenbo Xu
Hongyan Yao
Zundong Yin
Dianke Yu
Hongjie Yu
Shicheng Yu
Ben Zhang
Jun Zhang
Liubo Zhang
Wenhua Zhao
Yanlin Zhao
Xiaoying Zheng
Maigeng Zhou
Xiaonong Zhou
Guihua Zhuang

Advisory Board

Director of the Advisory Board Jiang Lu
Vice-Director of the Advisory Board Yu Wang Jianjun Liu Jun Yan

Members of the Advisory Board

Chen Fu
Gauden Galea (Malta)
Dongfeng Gu
Qing Gu
Yan Guo
Ailan Li
Jiafa Liu
Peilong Liu
Yuanli Liu
Kai Lu
Roberta Ness (USA)
Guang Ning
Minghui Ren
Chen Wang
Hua Wang
Kean Wang
Xiaoqi Wang
Zijun Wang
Fan Wu
Xianping Wu
Jingjing Xi
Jianguo Xu
Gonghuan Yang
Tilahun Yilma (USA)
Guang Zeng
Xiaopeng Zeng
Yonghui Zhang
Bin Zou

Editorial Office

Directing Editor Chihong Zhao
Managing Editors Yu Chen
Senior Scientific Editors Daxin Ni Ning Wang Wenwu Yin Shicheng Yu Jianzhong Zhang Qian Zhu

Scientific Editors

Weihong Chen
Tao Jiang
Xudong Li
Nankun Liu
Liwei Shi
Liuying Tang
Meng Wang
Zhihui Wang
Qi Yang
Qing Yue
Lijie Zhang
Ying Zhang

Cover Photo: credited from Dr. Zhujun Shao from National Institute for Communicable Disease Control and Prevention, China CDC.

Preplanned Studies

Emergence of Erythromycin-Resistant and Pertactin- and Filamentous Hemagglutinin-Deficient *Bordetella pertussis* Strains — Beijing, China, 2022–2023

Guilan Zhou[1,&]; Ying Li[2,&]; Hairui Wang[1]; Yuanyuan Wang[2]; Yuan Gao[1]; Juan Xu[1]; Fengshuang Wang[2];
Tao Peng[2]; Maojun Zhang[1]; Zhujun Shao[1,#]

Summary

What is already known about this topic?

Pertussis has reemerged as a significant public health threat, primarily due to variations in *Bordetella pertussis* strains, antimicrobial resistance, and vaccine evasion.

What is added by this report?

All isolated strains were identified as *ptxA1/ptxC2/ptxP3/prn150/fim2-1/fim3-1/fhaB1/tcfA2* type and exhibited resistance to erythromycin. Two strains showed a deficiency in Fha, thirty in Prn, and one strain exhibited multiple immunogen deficiencies.

What are the implications for public health practice?

The emergence and spread of immunogen-deficient strains likely result from prolonged vaccine selection pressure, posing challenges to the efficacy of pertussis vaccines. Additionally, the ongoing dissemination of *ptxP3* strains with high-level macrolide resistance presents a significant obstacle to clinical treatment strategies.

Pertussis, commonly known as whooping cough, is attributable to the Gram-negative bacterium *Bordetella pertussis*. Vaccination options against *B. pertussis* include whole-cell pertussis (wP) and acellular pertussis (aP) vaccines. Acellular vaccines typically consist of purified proteins from *B. pertussis*, especially filamentous hemagglutinin (Fha), pertussis toxin (Ptx), and pertactin (Prn), and often include fimbrial proteins (Fim2 and Fim3). During the 1990s, several countries recommended substituting the less reactive aP vaccines for wP vaccines (*1*). In China, the National Immunization Program has been administering the diphtheria–tetanus–wP vaccine since the 1980s. A shift to the diphtheria–tetanus–aP (DTaP) vaccine, which incorporates Ptx, Prn and Fha as bioactive components, occurred between 2007 and 2013 (*2*).

The resurgence of pertussis poses a significant global public health challenge, primarily due to vaccine escape and antigenic shifts in *Bordetella pertussis*. There has been a noted divergence in the antigens of *B. pertussis* between the strains circulating in the population and those present in vaccines (*3–4*). Strains exhibiting a novel promoter for Ptx (*ptxP3*) have been identified in various countries, including China (*5–7*). Significant virulence factors such as Prn and Fha, both integral components of *B. pertussis* vaccines, have shown variations. The first report of Prn-deficient *B. pertussis* strains occurred in the USA in 1994 (*4*), with similar strains later identified in China in 2019 (*8*). Instances of Fha-deficient *B. pertussis* strains have also been documented. Additionally, there has been a rise in the occurrence of high-level macrolide-resistant *B. pertussis* strains, particularly in China since 2013, which is linked to the A2037G mutation in the 23S rRNA gene (*5–6*).

Since 2022, two Beijing-based sentinel hospitals have implemented a pertussis surveillance study, monitoring cases suspected of pertussis and conducting laboratory tests for *B. pertussis* using real-time PCR from January 2022 to December 2023. A total of 44 *B. pertussis* strains were isolated from nasopharyngeal swab specimens collected from 44 outpatients, consisting of 13 infants, 28 children, and 3 adults. These strains underwent genetic analysis through sequencing using the Illumina HiSeq 2500 system. This analysis focused on genes encoding eight vaccine-related antigens (*ptxA, ptxC, ptxP3, prn, fim2, fim3, fhaB,* and *tcfA*) and a type III secretion system gene (*bscI*), analyzed using BLAST with an E-value threshold of 1e–5. Allelic variations for *ptxA, ptxC, ptxP3, prn, fim2-1, fim3-1, fhaB, tcfA2,* and *bscI* were identified through comparison on the BIGSdb-Pasteur platform (https://bigsdb.pasteur.fr/cgi-bin/bigsdb/bigsdb.pl?db=pubmlst_bordetella_seqdef). All identified *Bordetella pertussis* strains shared the same antigenic profile: *ptxA1, ptxC2, ptxP3, prn150, fim2-1, fim3-1, fhaB1, tcfA2,* and *bscI2.*

Notably, 14 strains had the *prn150* allele located on the same DNA sequence contig, whereas in the remaining 30 strains, this allele was split across two contigs due to a gene disruption at a site 240 bp upstream from the *prn* start site, identified as a common Prn-deficiency mechanism (*4*). This disruption was characterized by a 6-bp (GCTAGA) overlap and was associated with a reversed insertion of IS481, hinted by a "CTAG" termination sequence (accession no. M22031)(Figure 1). This insertion's location and orientation were confirmed by third-generation sequencing for two strains, one with an intact *prn150* (BJSY2023BRK008) and one with a truncated *prn150* (BJSY2022BRK001), performed on the PacBio platform. The completed genome of BJSY2022BRK001 confirmed reversed IS481 insertion in *prn* (Figure 2). Additionally, two strains showed a Fha deficiency, evidenced by a deletion of a "G" at position 1087 in the homopolymeric G-tract of *fhaB*, a mutation previously documented for causing this deficiency (*3*).

All *Bordetella pertussis* strains possessed identical 23S rRNA gene sequences and exhibited an A2037G mutation. Susceptibility testing conducted with E-test strips indicated that all strains were resistant to erythromycin and azithromycin, with minimum inhibitory concentrations (MIC) exceeding 256 μg/mL.

A phylogenetic tree was constructed based on core SNPs from 148 *B. pertussis* genomes. This set includes genomes from all strains analyzed in this study, two reference genomes (Tohama I, NC002929.2 and CS, CP086368), and an additional 102 genomes sourced from the NCBI database (BioProject no. PRJNA908268). The analysis revealed no specific linkage among the 44 isolated strains (Figure 3).

DISCUSSION

Pertussis, a disease preventable by vaccination, has seen an increase in global incidence even with high vaccination coverage; for instance, coverage for the diphtheria-tetanus-pertussis (DTaP) vaccine in China is reported at 99% (*7*). The DTaP vaccines used in China comprise *Bordetella pertussis* strains with the antigenic composition of *ptxA2/ptxC1/ptxP1/prn1/fim2-1/fim3-1/fhaB1/tcfA2*. Recent studies have indicated shifts in the primary vaccine antigens of *B. pertussis* compared to the vaccine strains. Li et al. identified the predominant virulence-associated genotype in northern China as *ptxA1/ptxC1/ptxP1/prn1/fim2-1/fim3A/tcfA2*, noting a rare occurrence of the *ptxP3* strains, all of which were sensitive to erythromycin (*6*). Fu et al. discovered that 41.1% of the highly virulent *B. pertussis* strains carried *ptxP3/prn2/ptxC2* and were all susceptible to macrolides, whereas the remaining 58.9% were less virulent, carrying *ptxP1/prn1/ptxC1* (*5*). All identified strains displayed the antigenic configuration *ptxA1/ptxC2/ptxP3/prn150/fim2-1/fim3-1/fhaB1/tcfA2* and *bscI2*, markedly diverging from the vaccine strain. Notably, all isolated strains contained *ptxP3/bscI2*, differing from previous studies that associated *ptxP3* strains with *bscI3* (*9*). Strains with *ptxP3* are reported to produce more Ptx than those with *ptxP1*, potentially indicating increased virulence (*10*). However, there are differing opinions on whether *ptxP1* strains might cause more severe diseases than *ptxP3* strains (*5*). Further research is necessary to elucidate the mechanisms driving the rapid proliferation of *ptxP3* strains in recent years.

Various mechanisms can result in Prn deficiency, such as mutations, deletions, and insertions within the *prn* gene. Cai et al. observed Prn-deficient strains in 11.7% of samples from Shanghai, characterized by

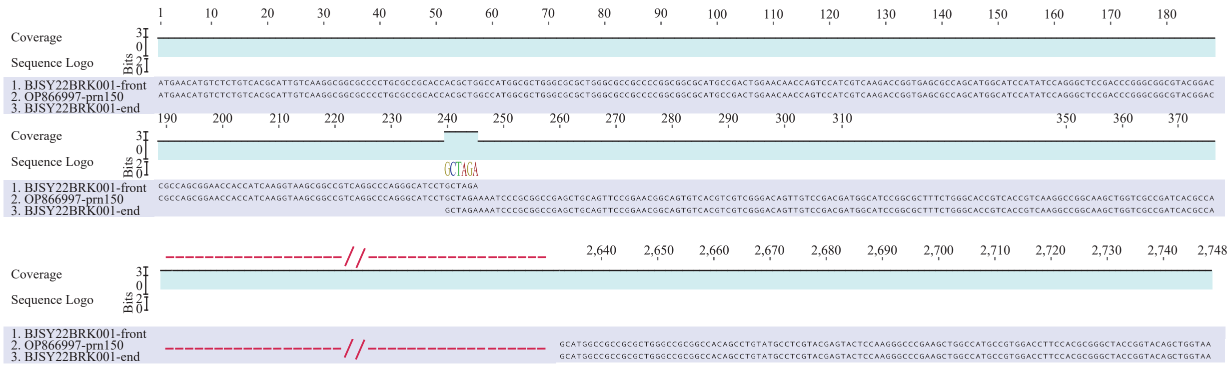

FIGURE 1. Comparison of the disrupted *prn* gene with the complete *prn150* allele, highlighting six overlapping bases (GCTAGA) between the contigs. OP866997-prn150: intact *prn150*.

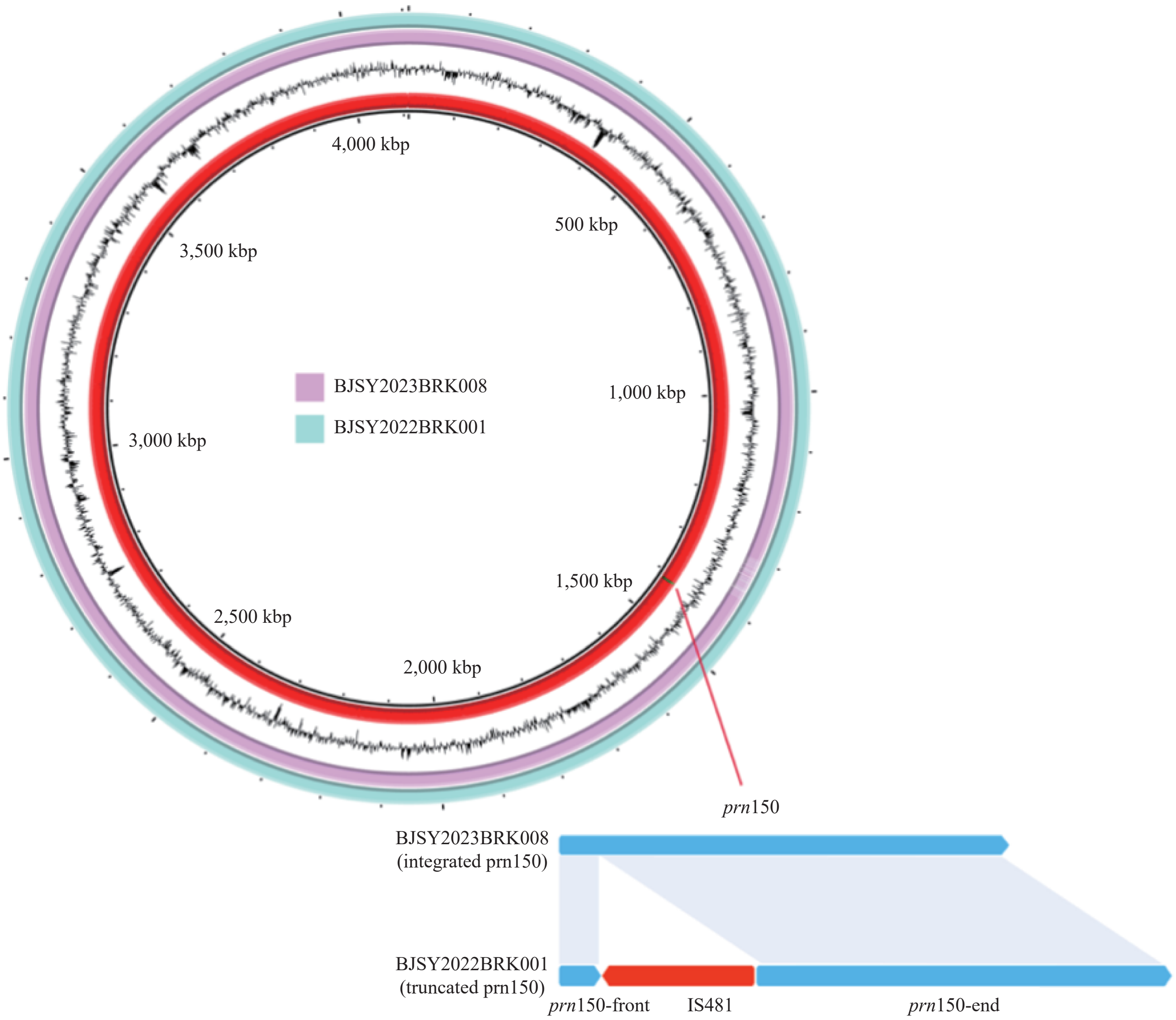

FIGURE 2. Circularized genomes featuring complete and truncated *prn150* genes. The purple ring denoted BJSY2023BRK008, while the light blue ring signified BJSY2022BRK001. The diagram illustrated the gene structures of complete *prn150* and *prn150* with a reversed IS481 insertion.

nucleotide deletions and stop codon mutations in *prn* (*7*). The insertion of IS481 was identified as the predominant cause of *prn* disruption (*4*). Another study reported that 100% of Prn-deficient isolates had Prn inactivated by IS481 insertion, which occurred independently across different *B. pertussis* lineages (*4*). In our research, we detected a high prevalence (68.2%, 30/44) of Prn-deficient *B. pertussis* strains resulting from IS481 insertion, representing the first documentation of such a significant occurrence.

Fha is a significant virulence factor of *B. pertussis*. In this study, we identified two strains deficient in Fha and one strain that was deficient in both Prn and Fha, marking the first reported cases of Fha-deficient strains in China. The emergence of strains with deficiencies in multiple immunogens poses an increasing public health concern, highlighting the necessity for ongoing surveillance of *B. pertussis* strains in China.

All *B. pertussis* strains examined in this study displayed resistance to macrolides, aligning with results from a recent study (*7*). The increasing prevalence of macrolide-resistant *B. pertussis* strains presents considerable challenges to clinical treatment.

The increasing dispersion of *ptxP3* strains, which are potentially more virulent and exhibit higher resistance to macrolides, poses substantial challenges for treating pertussis. Given the widespread prevalence of Prn-deficiency and the emergence of Fha-deficient *B. pertussis* strains, the development of vaccines by numerous local manufacturers is complicated, as Prn

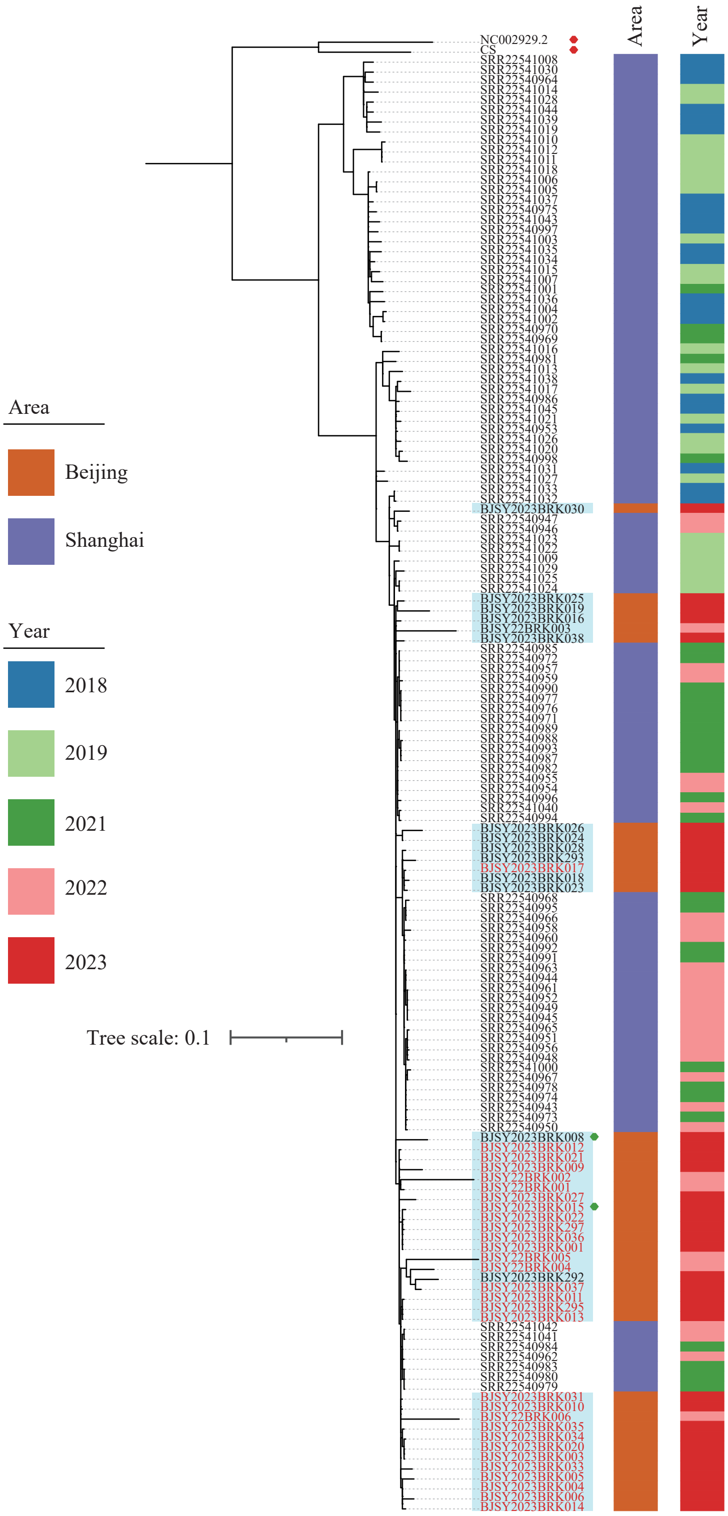

FIGURE 3. Phylogenetic tree based on core SNPs from *Bordetella pertussis*. The genome highlighted with a light blue background was sequenced in this study, and red fonts were Prn-deficient strains. Genomes marked with a red and green hexagon represented vaccine and Fha-deficient strains, respectively. The strains isolated during this study were distributed across various clusters within the tree.

Abbreviation: SNP=Single Nucleotide Polymorphism.

and Fha are key antigens in these vaccines. Selecting the appropriate pertussis vaccine for inclusion in China's National Immunization Program is crucial to enhancing the efficacy of pertussis prevention and control strategies.

The analysis in this study encompassed a limited number of strains, underscoring the need for ongoing surveillance of pertussis pathogens. In addition, only the genotypes of vaccine-associated antigens of isolated strains were analyzed in this study. The subsequent research on the function and pathogenic mechanism of antigen proteins is crucial for the evaluation of vaccine effectiveness and the development of vaccines.

Conflicts of interest: No conflicts of interest.

Acknowledgements: The staff of the participating hospitals and colleagues at Shunyi CDC.

Funding: Supported by the National Key Research and Development Program of China (grant number 2021YFC2301000) and the National Natural Science Foundation of China (NSFC) (grant number 81973106).

doi: 10.46234/ccdcw2024.085

Corresponding author: Zhujun Shao, shaozhujun@icdc.cn.

---

[1] National Key Laboratory of Intelligent Tracking and Forecasting for Infectious Diseases, National Institute for Communicable Disease Control and Prevention, Chinese Center for Disease Control and Prevention, Beijing, China; [2] Shunyi District Center for Disease Control and Prevention, Beijing, China.
& Joint first authors.

Submitted: February 05, 2024; Accepted: May 09, 2024

REFERENCES

1. Mattoo S, Cherry JD. Molecular pathogenesis, epidemiology, and clinical manifestations of respiratory infections due to *Bordetella pertussis* and other *Bordetella subspecies*. Clin Microbiol Rev 2005;18(2):326 – 82. https://doi.org/10.1128/CMR.18.2.326-382.2005.
2. Long Z, Wei C, Zhan ZQ, Ma X, Li XL, Li YQ, et al. Quantitative determination of bioactive proteins in diphtheria tetanus acellular pertussis (DTaP) vaccine by liquid chromatography tandem mass spectrometry. J Pharm Biomed Anal 2019;169:30 – 40. https://doi.org/10.1016/j.jpba.2019.02.029.
3. Weigand MR, Pawloski LC, Peng YH, Ju H, Burroughs M, Cassiday PK, et al. Screening and genomic characterization of filamentous hemagglutinin-deficient *Bordetella pertussis*. Infect Immun 2018;86(4): e00869 – 17. https://doi.org/10.1128/IAI.00869-17.
4. Pawloski LC, Queenan AM, Cassiday PK, Lynch AS, Harrison MJ, Shang W, et al. Prevalence and molecular characterization of pertactin-deficient *Bordetella pertussis* in the United States. Clin Vaccine Immunol 2014;21(2):119 – 25. https://doi.org/10.1128/CVI.00717-13.
5. Fu P, Wang CQ, Tian H, Kang ZH, Zeng M. *Bordetella pertussis* infection in infants and young children in Shanghai, China, 2016-2017: clinical features, genotype variations of antigenic genes and macrolides resistance. Pediatr Infect Dis J 2019;38(4):370 – 6. https://doi.org/10.1097/INF.0000000000002160.
6. Li LJ, Deng JK, Ma X, Zhou K, Meng QH, Yuan L, et al. High prevalence of macrolide-resistant *Bordetella pertussis* and *ptxP1* genotype, Mainland China, 2014-2016. Emerg Infect Dis 2019;25(12): 2205 – 14. https://doi.org/10.3201/eid2512.181836.
7. Cai JH, Chen ML, Liu QY, Luo JY, Yuan LY, Chen YX, et al. Domination of an emerging erythromycin-resistant *ptxP3 Bordetella pertussis* clone in Shanghai, China. Int J Antimicrob Agents 2023;62(1): 106835. https://doi.org/10.1016/j.ijantimicag.2023.106835.
8. Xu Z, Wang ZG, Luan Y, Li YR, Liu XG, Peng XK, et al. Genomic epidemiology of erythromycin-resistant *Bordetella pertussis* in China. Emerg Microbes Infect 2019;8(1):461 – 70. https://doi.org/10.1080/22221751.2019.1587315.
9. Xu Z, Hu DL, Luu LDW, Octavia S, Keil AD, Sintchenko V, et al. Genomic dissection of the microevolution of Australian epidemic *Bordetella pertussis*. Emerg Microbes Infect 2022;11(1):1460 – 73. https://doi.org/10.1080/22221751.2022.2077129.
10. Mooi FR, van Loo IHM, van Gent M, He QS, Bart MJ, Heuvelman KJ, et al. *Bordetella pertussis* strains with increased toxin production associated with pertussis resurgence. Emerg Infect Dis 2009;15(8): 1206 – 13. https://doi.org/10.3201/eid1508.081511.

Vital Surveillances

Evolutionary Diversity of Coxsackievirus A6 Causing Severe Hand, Foot, and Mouth Disease — China, 2012–2023

Huanhuan Lu[1]; Jinbo Xiao[1]; Wenhui Wang[2]; Dongmei Yan[1]; Tianjiao Ji[1]; Qian Yang[1]; Haiyan Wei[3]; Yanhua Du[4];
Yunting Zeng[5]; Jun Guo[6]; Jianhua Chen[7]; Hanri Zeng[8]; Yingying Liu[9]; Shuaifeng Zhou[10]; Hong Ji[11];
Jianxing Wang[12]; Xiaofang Zhou[13]; Yong Zhang[1,#]

ABSTRACT

Introduction: Coxsackievirus A6 (CVA6) has emerged as a significant pathogen responsible for severe cases of hand, foot, and mouth disease (HFMD). This study aims to delineate the demographic characteristics and analyze the viral evolution of severe HFMD associated with CVA6, thereby assisting in its surveillance and management.

Methods: In this investigation, 74 strains of CVA6 were isolated from samples collected from severe HFMD cases between 2012 and 2023. The *VP1* gene sequences of CVA6 were amplified and analyzed to assess population historical dynamics and evolutionary characteristics using BEAST, DnaSP6, and PopART.

Results: A significant portion (94.4%) of severe CVA6-associated HFMD cases (51 out of 54, with 20 lacking age information) were children under 5 years old. Among the 74 CVA6 strains analyzed, 72 belonged to the D3a sub-genotype, while only two strains were D2 sub-genotype. The average genetic distance between *VP1* sequences prior to 2015 was 0.027, which increased to 0.051 when compared to sequences post-2015. Historical population dynamics analysis indicated three significant population expansions of severe CVA6-associated HFMD during 2012–2013, 2013–2014, and 2019–2020, resulting in the formation of 65 distinct haplotypes. Consistent with the MCC tree findings, transitioning between regional haplotypes required multiple base substitutions, showcasing an increase in population diversity during the evolutionary process (from 14 haplotypes in 2013 to 55 haplotypes over the subsequent decade).

Conclusions: CVA6, associated with severe HFMD, is evolving and presents a risk of outbreak occurrence. Thus, enhanced surveillance of severe HFMD is imperative.

Hand, foot, and mouth disease (HFMD) is a contagious disease predominantly caused by several enteroviruses and primarily affects infants and children (*1*). Typically characterized by fever, mouth ulcers, and rash, HFMD symptoms are often mild and generally resolve within 7–10 days. However, some individuals may develop severe symptoms such as fever, a stiff neck, shortness of breath, and worsening rash, leading to potentially life-threatening neurological, respiratory, or circulatory complications, including aseptic meningitis, encephalitis, acute flaccid paralysis, pulmonary hemorrhage, pulmonary edema, and cardiopulmonary failure (*2*). HFMD was classified as a notifiable disease in May 2008, identifying enterovirus A71 (EV-A71) as the predominant pathogen responsible for severe and fatal cases (*3*). The widespread administration of an inactivated EV-A71 vaccine in 2016 significantly decreased the incidence of EV-A71-associated HFMD cases (*4*). Nevertheless, the diversity of pathogens leading to severe HFMD has evolved recently due to the absence of cross-protection among different enterovirus serotypes (*5*). Coxsackievirus A6 (CVA6) has emerged as the primary pathogen in severe HFMD cases across various regions in China. For instance, in 2013, the Third People's Hospital of Shenzhen reported that all eight patients with severe HFMD tested positive for CVA6, all developing meningitis, with two also suffering myocardial damage (*6*). Similarly, in 2017, the Guangdong Women and Children's Hospital found that among 55 patients with CVA6-associated severe HFMD, 29 (52.7%) developed aseptic meningitis, and six (10.9%) also experienced pulmonary edema (*7*).

Enteroviruses possess a single-stranded, positive-sense RNA genome that encodes both structural and nonstructural viral proteins. After entering a cell, the genomic RNA translates into a polyprotein divided into three regions: P1, P2, and P3. This polyprotein is then segmented into individual proteins by viral proteases. Specifically, the P1 region comprises four structural proteins (*VP1*–*VP4*) (*8*). Variations in the nucleotide sequences of the *VP1* region are utilized for molecular typing of enteroviruses (*9*). Studies focusing on the molecular typing of CVA6 based on these sequences have identified the D3 sub-genotype as the predominant strain globally since 2008, with the D3a sub-genotype being the most widespread in China (*5*).

Based on the national laboratory surveillance network for HFMD pathogens established in the Chinese mainland in 2008, a total of 74 CVA6 strains were obtained from severe HFMD cases between 2012 and 2023. Analysis of their *VP1* sequences allowed for the inference of the population's historical dynamics and the evolutionary characteristics of CVA6. This study aims to provide insights into the surveillance of severe HFMD cases.

METHODS

Case Inclusion Criteria

According to the HFMD Treatment Guidelines (2010 and 2018 editions), severe HFMD cases were defined by the following clinical signs: persistent high fever (>39 °C), neurological symptoms (depression and abnormal movement), atypical respiratory symptoms (abnormalities in respiratory rate), and circulatory dysfunction (abnormal heart rate and prolonged capillary refill time). Cases that met these criteria were included in the study, which aimed to enhance public health surveillance and informed decision-making without involving human experimentation. The study received approval from the Second Ethics Review Committee of the National Institute for Viral Disease Control and Prevention at the Chinese Center for Disease Control and Prevention.

Sample Collection and Viral Isolation

According to surveillance guidelines, the local CDC collected samples (e.g., stool and throat swabs) from severe HFMD cases and transported them to designated laboratories for EVs screening using Real-time RT-PCR. All CVA6-positive samples were subsequently forwarded to the provincial CDC for virus isolation following the standard protocol (Polio Laboratory Manual, 4th ed, https://iris.who.int/handle/10665/68762). The National Polio Laboratory at the National Institute of Viral Disease Prevention and Control in China was tasked with genotype identification.

Molecular Typing of Enteroviruses

Nucleic acid extraction from cell cultures was carried out using the Tianlong nucleic acid extraction kit (Ex-DNA/RNA Virus (CDC)/T327, Xi'an Tianlong Technology Co., Ltd., China) and the GeneRotex 96 nucleic acid extractor (Xi'an Tianlong Technology Co., Ltd., China). The *VP1* coding region was amplified through reverse transcription polymerase chain reaction (RT-PCR) utilizing the PrimeScript One Step RT-PCR kit version 2 (RR057A, TaKaRa, China). Specific primers for amplification included CVA6-2339Y (5'–3': CCTTCTGAGGCCAACA TCAT) and CVA6-3461Z (5'–3': ATACCAAGTTGG CCCAGTCA). Sequencing was conducted using an ABI 3130 genetic analyzer (Applied Biosystems, Foster City, CA, USA), and data analysis was performed using Sequencher software (version 5.4.6, Ann Arbor, USA) to determine the *VP1* coding sequence of enteroviruses. Molecular typing of sequences was completed via the enterovirus typing tool available at www.rivm.nl/mpf/enterovirus/typingtool.

Inference of Population Historical Dynamics

The alignment of sequences was performed using MAFFT software (version 7.490) (*10*), while the best nucleotide substitution model was identified using ModelGenerator (version 0.85). RAxML-NG (version 0.9.0) was utilized to construct the maximum likelihood phylogenetic tree (*11*). TempEst (version 1.5) facilitated the analysis of the temporal structure of the sequences (*12*). The optimal molecular clock model and tree prior were determined through Path Sampling/Stepping-stone techniques (*13*). Bayesian phylogenetic analysis was executed using BEAST (version 1.8.4) (*14*), with the analysis outputs reviewed in Trace software (version 1.7.1). The Bayesian maximum clade credibility (MCC) tree was constructed using TreeAnnotator (version 1.8.4) and visualized in FigTree software (version 1.4) (http://tree.bio.ed.ac.uk/software/). A single haplotype was defined in DnaSP6 software (version 6.12.03) (*15*) when nucleotide sequences were identical, aiding in the understanding of nucleotide mutations throughout viral evolution. The median-joining haplotype network was built using PopART software (version 1.7).

RESULTS

Demographic Characteristics of HFMD Cases with CVA6 Infections

This study analyzed 74 CVA6 strains isolated from severe HFMD cases, which were submitted by provincial HFMD surveillance laboratories between 2012 and 2023. Of the 74 CVA6-associated severe HFMD cases, 48 were in males and 26 in females. The patients had a median age of 2.0 years (mean age 2.05 years, range 6 months to 6.5 years). The age distribution was as follows: 25 cases in children under 1 year old, 26 cases in those aged 1–5 years, and three cases in children older than 5 years (Table 1).

CVA6 isolates identified in 97.3% (72/74) of cases were predominantly of the D3a sub-genotype, while the D2 sub-genotype was solely found in Northwest China (Figure 1). The cases were primarily located in Central and Western China, with the most cases reported in Northwest China (25 cases), followed by Central China (22 cases), South China (13 cases), Southwest China (8 cases), North China (4 cases), and East China (2 cases). Incidences before 2015 were predominantly in Northwest China, whereas occurrences post-2015 were mainly in Central, South, and Southwest China (Table 1).

Inference of Population Historical Dynamics

The MCC tree analysis revealed that CVA6 sequences from the same geographical region displayed high similarity and often clustered together. Regarding the temporal distribution of CVA6 in severe HFMD cases, sampling in Northwest China was primarily conducted before 2015. In contrast, post-2015 samples predominantly came from patients with severe HFMD in Central, South, and Southwest China. The evolutionary distances between post-2015 sequences and those isolated earlier in Northwest China significantly increased. Specifically, the average genetic distance was 0.027 for sequences before 2015 and increased to 0.051 for sequences post-2015 compared to earlier sequences (Figure 2A). Within the same region, the average genetic distance among sequences was 0.032, whereas it was 0.044 between different regions (Figure 2B). Furthermore, Bayesian skyline plot analysis indicated that the D3a sub-genotype of CVA6, isolated from 72 cases, experienced three population expansions during its evolutionary history, specifically in 2012–2013, 2013–2014, and 2019–2020. Notably, there were significant increases in the population size during the periods 2012–2013 and 2019–2020 (Figure 2C).

Analysis of the 72 CVA6 D3a *VP1* sequences identified 258 variable sites within the 915 bp fragment, encompassing 65 haplotypes. In 2013, there were 14 haplotypes, with 41 additional haplotypes emerging over the subsequent decade. Of the 65 haplotypes, 58 (89.2%, 58/65) comprised solely a single sequence. These haplotypes were distributed across various regions, forming several large clusters of regionally originated haplotypes in the haplotype network plot and the MCC tree. This clustering indicates that haplotypes from different regions diverged through multiple base substitutions. The analyses also imply the existence of further undetected samples, as evidenced in Figure 2D and Table 1.

DISCUSSION

Unlike mild HFMD, severe cases can lead to neurological, respiratory, or circulatory complications, and treatment delays may result in further deterioration. EV-A71 has been identified as the predominant pathogen responsible for severe HFMD. However, following the introduction of the inactivated EV-A71 vaccine in 2016, the spectrum of pathogens causing HFMD has shifted, with other enteroviruses, particularly CVA6, emerging as the primary causative agents (*5*).

Seventy-four cases of severe HFMD associated with CVA6 were reported in children under the age of 5 years. The immature immune systems of this age group may heighten their susceptibility, leading to severe complications and potentially fatal outcomes if not promptly diagnosed and treated (*2*). Consequently, the development and administration of vaccines targeting CVA6 are crucial to prevent severe HFMD in susceptible children.

The CVA6 genotype, particularly the dominant D3a sub-genotype in China, has been isolated primarily, with only two instances of the D2 strain identified in 2013. This underscores the necessity for ongoing robust surveillance of severe HFMD specifically targeting the CVA6 D3a sub-genotype. In this study, a total of 74 CVA6 strains were collected from severe HFMD cases between 2012 and 2023, predominantly in Central China, Northwest China, and South China. It is important to note that the limited number of samples and the considerable variability in surveillance quality across provinces may introduce bias in the

TABLE 1. Summary of information on 74 cases of CVA6-associated severe hand, foot, and mouth disease in China, 2012–2023.

Patient number	Gender	Age (years)	Region	Year	Haplotype	Sub-genotype	NMDC number
HFMD1	Female	1	Northwest China	2018	Hap_41	D3a	NMDCN00038LF
HFMD2	Male	1	Northwest China	2017	Hap_37	D3a	NMDCN00038L8
HFMD3	Female	2	Northwest China	2015	Hap_42	D3a	NMDCN00038LI
HFMD4	Male	4	Northwest China	2015	Hap_43	D3a	NMDCN00038LJ
HFMD5	Female	3	Northwest China	2015	Hap_29	D3a	NMDCN00038JS
HFMD6	Female	1	South China	2021	Hap_48	D3a	NMDCN00038K8
HFMD7	Male	2	South China	2023	Hap_56	D3a	NMDCN00038LH
HFMD8	Female	2	South China	2023	Hap_57	D3a	NMDCN00038LN
HFMD9	Male	2	South China	2023	Hap_58	D3a	NMDCN00038LQ
HFMD10	Male	4	South China	2020	Hap_47	D3a	NMDCN00038K5
HFMD11	Male	2	Southwest China	2022	Hap_62	D3a	NMDCN00038LU
HFMD12	Male	4	Southwest China	2022	Hap_63	D3a	NMDCN00038LV
HFMD13	Male	4	Southwest China	2022	Hap_63	D3a	NMDCN00038M0
HFMD14	Male	3	Southwest China	2022	Hap_64	D3a	NMDCN00038M1
HFMD15	Female	1	Southwest China	2022	Hap_60	D3a	NMDCN00038LR
HFMD16	Male	2	Southwest China	2022	Hap_61	D3a	NMDCN00038LS
HFMD17	Female	2	Southwest China	2020	Hap_59	D3a	NMDCN00038LC
HFMD18	Female	5	South China	2018	Hap_54	D3a	NMDCN00038KS
HFMD19	Female	<1	South China	2018	Hap_55	D3a	NMDCN00038KT
HFMD20	Female	2	South China	2018	Hap_55	D3a	NMDCN00038KU
HFMD21	Male	1	South China	2018	Hap_53	D3a	NMDCN00038KR
HFMD22	Female	2	South China	2018	Hap_51	D3a	NMDCN00038KM
HFMD23	Female	1	South China	2018	Hap_52	D3a	NMDCN00038KN
HFMD24	Male	5	South China	2018	Hap_49	D3a	NMDCN00038KK
HFMD25	Male	2	South China	2018	Hap_50	D3a	NMDCN00038KL
HFMD26	Male	<1	North China	2017	Hap_25	D3a	NMDCN00038KO
HFMD27	Female	<1	North China	2017	Hap_26	D3a	NMDCN00038KQ
HFMD28	Male	2	North China	2017	Hap_24	D3a	NMDCN00038KJ
HFMD29	Male	1	North China	2015	Hap_23	D3a	NMDCN00038K2
HFMD30	Male	1	Central China	2019	Hap_14	D3a	NMDCN00038L3
HFMD31	Male	/[*]	Central China	2020	Hap_6	D3a	NMDCN00038K3
HFMD32	Female	–	Central China	2020	Hap_12	D3a	NMDCN00038L0
HFMD33	Male	–	Central China	2020	Hap_9	D3a	NMDCN00038KB
HFMD34	Male	–	Central China	2020	Hap_10	D3a	NMDCN00038KC
HFMD35	Male	–	Central China	2020	Hap_11	D3a	NMDCN00038KP
HFMD36	Female	–	Central China	2020	Hap_3	D3a	NMDCN00038JU
HFMD37	Male	–	Central China	2020	Hap_4	D3a	NMDCN00038JV
HFMD38	Male	–	Central China	2020	Hap_5	D3a	NMDCN00038K1
HFMD39	Male	–	Central China	2020	Hap_7	D3a	NMDCN00038K4
HFMD40	Male	–	Central China	2020	Hap_7	D3a	NMDCN00038K6
HFMD41	Male	–	Central China	2020	Hap_8	D3a	NMDCN00038K9
HFMD42	Male	–	Central China	2020	Hap_1	D3a	NMDCN00038JR

Continued

Patient number	Gender	Age (years)	Region	Year	Haplotype	Sub-genotype	NMDC number
HFMD43	Male	−	Central China	2020	Hap_15	D3a	NMDCN00038L4
HFMD44	Male	−	Central China	2020	Hap_17	D3a	NMDCN00038L9
HFMD45	Male	−	Central China	2020	Hap_18	D3a	NMDCN00038LD
HFMD46	Male	−	Central China	2020	Hap_19	D3a	NMDCN00038LG
HFMD47	Female	−	Central China	2020	Hap_20	D3a	NMDCN00038LK
HFMD48	Female	−	Central China	2020	Hap_20	D3a	NMDCN00038LO
HFMD49	Male	−	Central China	2020	Hap_13	D3a	NMDCN00038L1
HFMD50	Female	6	Central China	2019	Hap_16	D3a	NMDCN00038L6
HFMD51	Male	4	Central China	2014	Hap_2	D3a	NMDCN00038JT
HFMD52	Male	4	East China	2017	Hap_21	D3a	NMDCN00038L7
HFMD53	Female	1	East China	2017	Hap_22	D3a	NMDCN00038LT
HFMD54	Female	3	Northwest China	2020	Hap_32	D3a	NMDCN00038KE
HFMD55	Male	4	Northwest China	2020	Hap_33	D3a	NMDCN00038KF
HFMD56	Male	<1	Northwest China	2013	Hap_35	D3a	NMDCN00038KH
HFMD57	Male	1	Northwest China	2013	Hap_45	D3a	NMDCN00038LM
HFMD58	Female	3	Northwest China	2013	Hap_39	D3a	NMDCN00038LB
HFMD59	Female	1	Northwest China	2013	Hap_36	D3a	NMDCN00038KI
HFMD60	Male	1	Northwest China	2013	Hap_32	D3a	NMDCN00038KD
HFMD61	Male	1	Northwest China	2013	Hap_31	D3a	NMDCN00038K7
HFMD62	Female	1	Northwest China	2013	Hap_30	D3a	NMDCN00038K0
HFMD63	Female	2	Northwest China	2013	Hap_46	D3a	NMDCN00038LP
HFMD64	Male	1	Northwest China	2013	Hap_44	D3a	NMDCN00038LL
HFMD65	Male	1	Northwest China	2013	Hap_40	D3a	NMDCN00038LE
HFMD66	Male	2	Northwest China	2013	Hap_38	D3a	NMDCN00038LA
HFMD67	Male	1	Northwest China	2013	Hap_37	D3a	NMDCN00038L5
HFMD68	Male	2	Northwest China	2013	Hap_34	D3a	NMDCN00038KG
HFMD69	Male	1	Northwest China	2013	/†	D2	NMDCN00038KA
HFMD70	Male	1	Northwest China	2013	−	D2	NMDCN00038L2
HFMD71	Male	1	Northwest China	2013	Hap_27	D3a	NMDCN00038JP
HFMD72	Female	1	Northwest China	2014	Hap_36	D3a	NMDCN00038KV
HFMD73	Female	2	Northwest China	2014	Hap_28	D3a	NMDCN00038JQ
HFMD74	Male	−	Southwest China	2021	Hap_65	D3a	NMDCN00038M2

Note: Northwest China includes Shaanxi, Gansu, and Qinghai provinces; and Ningxia Hui Autonomous Region and Xinjiang Uygur Autonomous Region. South China includes Guangdong and Hainan provinces; Guangxi Zhuang Autonomous Region; and Hong Kong SAR and Macao SAR. Southwest China includes Sichuan, Guizhou, and Yunnan provinces; Chongqing Municipality; and Xizang Autonomous Region. North China includes Hebei and Shanxi provinces; Beijing and Tianjin Municipality; and Inner Mongolia Autonomous Region. Central China includes Henan, Hubei, and Hunan provinces. East China includes Jiangsu, Zhejiang, Anhui, Fujian, Jiangxi, and Shandong provinces; Shanghai Municipality; and Taiwan, China.

Abbreviation: HFMD=hand, foot and mouth disease; SAR=Special Administrative Region.

* Missing age information for this case;

† No haplotype analysis of D2.

analysis, potentially skewing the true prevalence of CVA6-associated severe HFMD.

D3a has been the predominant sub-genotype of CVA6 in China since 2012. Population dynamic analyses reveal that the virus isolated from severe HFMD cases exhibited three major expansions, reflecting increased diversity within the CVA6 population post-2012. Haplotype reconstruction from 74 sequences identified 65 unique haplotypes, underscoring the extensive diversity among CVA6

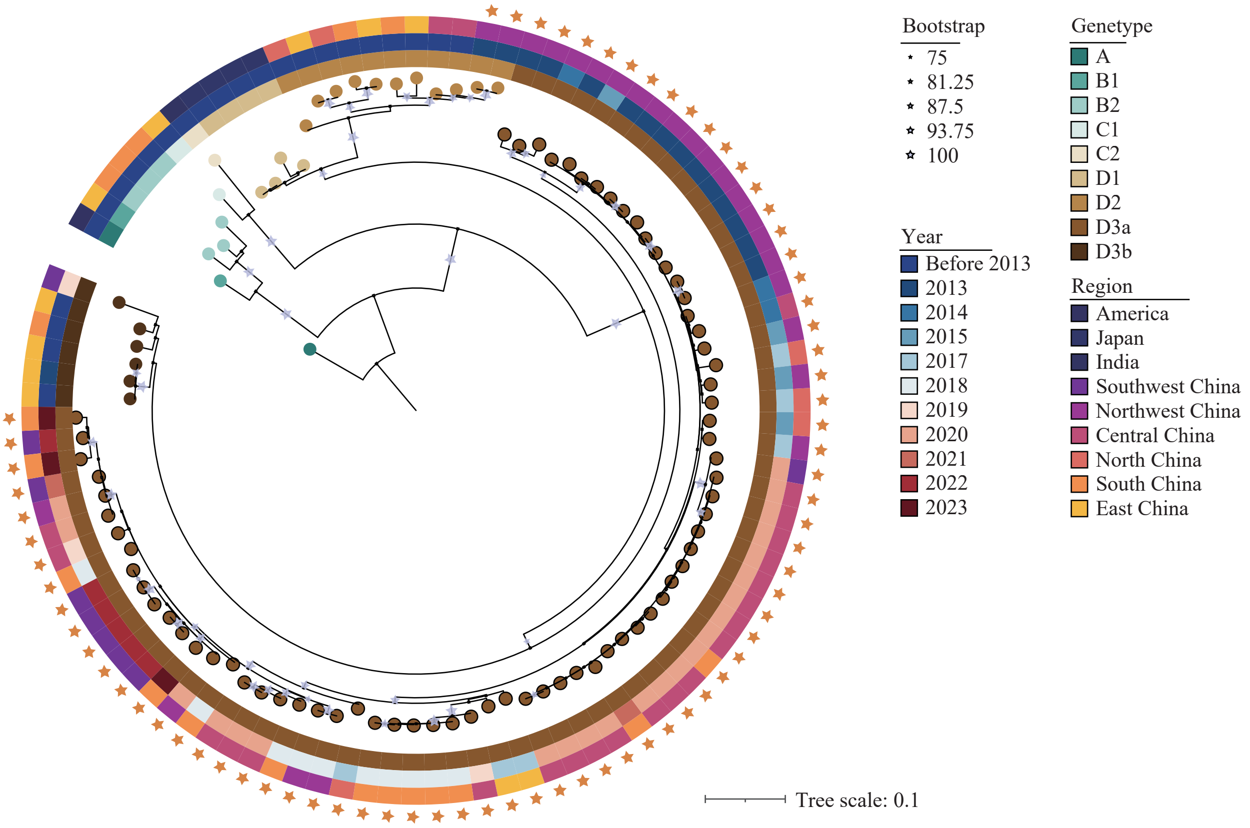

FIGURE 1. Molecular typing of 74 CVA6 strains isolated from severe HFMD in China, 2012–2023. The ML tree, constructed using the VP1 coding region, was utilized to determine the genotype of the CVA6 strains isolated in this study.
Abbreviation: CVA6=Coxsackievirus A6; HFMD=hand, foot, and mouth disease; ML=maximum likelihood.

strains associated with severe HFMD across different regions. Notably, no shared haplotypes were found between regions, suggesting the existence of undetected haplotypes and potentially unmonitored severe HFMD cases associated with CVA6. Current diagnostic criteria for severe HFMD, which include mild clinical symptoms with neurological or circulatory complications (*2*), may lead to misdiagnoses, such as enteroviral meningitis, thus contributing to the underreporting of severe HFMD cases. Given these findings, enhancing surveillance and improving clinician training on the identification and reporting of severe HFMD is essential to better assess and manage the disease burden.

Conflicts of interest: No conflicts of interest.

Acknowledgements: The staff of the local Centers for Disease Control and Prevention in Gansu, Guangdong, Guizhou, Hainan, Hebei, Henan, Hunan, Jiangsu, Shandong, Shaanxi, Sichuan, Yunnan, Zhejiang, and Chongqing PLADs for their efforts in collecting the clinical samples.

Funding: Supported by the Beijing Natural Science Foundation (L234052) and the National Key Research and Development Program of China (2021YFC2302003).

doi: 10.46234/ccdcw2024.086

Corresponding author: Yong Zhang, yongzhang75@sina.com.

---

[1] National Key Laboratory of Intelligent Tracking and Forecasting for Infectious Diseases; World Health Organization Polio Reference Laboratory for the Western Pacific Region; Key Laboratory of Laboratory Biosafety, National Health and Key Laboratory of Laboratory Biosafety of the National Health Commission, National Institute for Viral Disease Control and Prevention, Chinese Center for Disease Control and Prevention, Beijing, China; [2] Linyi Center for Disease Control and Prevention, Linyi City, Shandong Province, China; [3] Henan Provincial Center for Disease Control and Prevention, Zhengzhou City, Henan Province, China; [4] Shaanxi Provincial Center for Disease Control and Prevention, Xi'an City, Shaanxi Province, China; [5] Hainan Provincial Center for Disease Control and Prevention, Haikou City, Hainan Province, China; [6] Guizhou Provincial Center for Disease Control and Prevention, Guiyang City, Guizhou Province, China; [7] Gansu Provincial Center for Disease Control and Prevention, Lanzhou City, Gansu Province, China; [8] Guangdong Provincial Center for Disease Control and Prevention, Guangzhou City, Guangdong Province, China; [9] Hebei Provincial Center for Disease Control and Prevention, Shijiazhuang City, Hebei Province, China; [10] Hunan Provincial Center for Disease Control and Prevention, Changsha City, Hunan Province, China; [11] Jiangsu Provincial Center for Disease Control and Prevention, Nanjing City, Jiangsu Province, China; [12] Shandong Provincial Center for Disease Control and Prevention, Jinan City, Shandong Province, China; [13] Yunnan Provincial Center for Disease Control and Prevention, Kunming City, Yunnan Province, China.

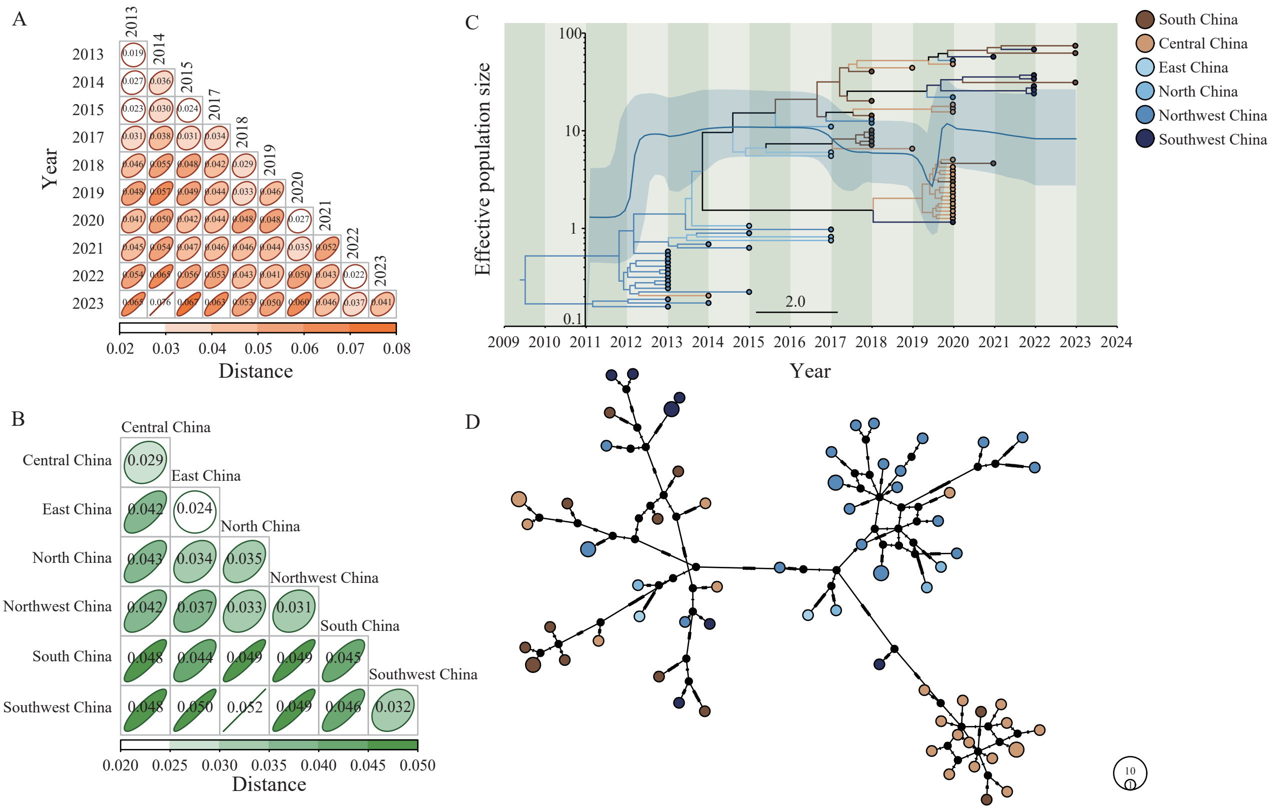

FIGURE 2. Inferred historical population dynamics of 74 CVA6 strains isolated from severe HFMD cases in China, 2012–2023. (A) Variation in nucleotide sequences of CVA6 from different regions. (B) Variation in nucleotide sequences of CVA6 across different years. (C) MCC tree and Bayesian skyline plot of the VP1 region of CVA6 depicting the 95% confidence intervals of the HPD analysis with light blue shading. Sequences from various regions are differentiated by color. (D) In the median-joining network, the circle size correlates with haplotype frequency, while unsampled haplotypes are shown as small black solid circles. Each connecting line indicates a mutational step between haplotypes.

Abbreviation: CVA6=Coxsackievirus A6; HFMD=Hand, foot, and mouth disease; MCC=Maximum clade credibility; HPD=Highest posterior density.

Submitted: February 02, 2024; Accepted: May 08, 2024

REFERENCES

1. Xu W, Liu CF, Yan L, Li JJ, Wang LJ, Qi Y, et al. Distribution of enteroviruses in hospitalized children with hand, foot and mouth disease and relationship between pathogens and nervous system complications. Virol J 2012;9:8. https://doi.org/10.1186/1743-422x-9-8.
2. Chong CY, Chan KP, Shah VA, Ng WYM, Lau G, Teo TES, et al. Hand, foot and mouth disease in Singapore: a comparison of fatal and non-fatal cases. Acta Paediatr 2003;92(10):1163-9.
3. Tan XJ, Huang XY, Zhu SL, Chen H, Yu QL, Wang HY, et al. The persistent circulation of enterovirus 71 in People's Republic of China: causing emerging nationwide epidemics since 2008. PLoS One 2011;6(9):e25662. https://doi.org/10.1371/journal.pone.0025662.
4. Xiao JB, Huang KQ, Lu HH, Song Y, Han ZZ, Zhang M, et al. Genomic epidemiology and phylodynamic analysis of enterovirus A71 reveal its transmission dynamics in Asia. Microbiol Spectr 2022;10(5):e0195822. https://doi.org/10.1128/spectrum.01958-22.
5. Song Y, Zhang Y, Han ZZ, Xu W, Xiao JB, Wang XJ, et al. Genetic recombination in fast-spreading coxsackievirus A6 variants: a potential role in evolution and pathogenicity. Virus Evol 2020;6(2):veaa048. https://doi.org/10.1093/ve/veaa048.
6. Yang F, Yuan J, Wang X, Li J, Du J, Su H, et al. Severe hand, foot, and mouth disease and coxsackievirus A6-Shenzhen, China. Clin Infect Dis 2014;59(10):1504 – 5. https://doi.org/10.1093/cid/ciu624.
7. Yang XH, Li YY, Zhang CB, Zhan WL, Xie J, Hu SQ, et al. Clinical features and phylogenetic analysis of severe hand-foot-and-mouth disease caused by Coxsackievirus A6. Infect Genet Evol 2020;77:104054. https://doi.org/10.1016/j.meegid.2019.104054.
8. Zhang Y, Hong M, Sun Q, Zhu SL, Tsewang N, Li XL, et al. Molecular typing and characterization of a new serotype of human enterovirus (EV-B111) identified in China. Virus Res 2014;183:75 – 80. https://doi.org/10.1016/j.virusres.2014.01.002.
9. Oberste MS, Maher K, Kilpatrick DR, Pallansch MA. Molecular evolution of the human enteroviruses: correlation of serotype with VP1 sequence and application to picornavirus classification. J Virol 1999;73(3):1941 – 8. https://doi.org/10.1128/jvi.73.3.1941-1948.1999.
10. Katoh K, Rozewicki J, Yamada KD. MAFFT online service: multiple sequence alignment, interactive sequence choice and visualization. Brief Bioinform 2019;20(4):1160 – 6. https://doi.org/10.1093/bib/bbx108.
11. Kozlov AM, Darriba D, Flouri T, Morel B, Stamatakis A. RAxML-NG: a fast, scalable and user-friendly tool for maximum likelihood phylogenetic inference. Bioinformatics 2019;35(21):4453 – 5. https://doi.org/10.1093/bioinformatics/btz305.
12. Rambaut A, Lam TT, Max Carvalho L, Pybus OG. Exploring the temporal structure of heterochronous sequences using TempEst (formerly Path-O-Gen). Virus Evol 2016;2(1):vew007. https://doi.org/10.1093/ve/vew007.
13. Baele G, Lemey P, Bedford T, Rambaut A, Suchard MA, Alekseyenko

AV. Improving the accuracy of demographic and molecular clock model comparison while accommodating phylogenetic uncertainty. Mol Biol Evol 2012;29(9):2157 – 67. https://doi.org/10.1093/molbev/mss084.

14. Drummond AJ, Suchard MA, Xie D, Rambaut A. Bayesian phylogenetics with BEAUti and the BEAST 1. 7. Mol Biol Evol 2012;29(8):1969 – 73. https://doi.org/10.1093/molbev/mss075.
15. Rozas J, Ferrer-Mata A, Sánchez-DelBarrio JC, Guirao-Rico S, Librado P, Ramos-Onsins SE, et al. DnaSP 6: DNA sequence polymorphism analysis of large data sets. Mol Biol Evol 2017;34(12):3299 – 302. https://doi.org/10.1093/molbev/msx248.

Vital Surveillances

Seasonal and Genetic Characteristics of Human Metapneumovirus Circulating — Henan Province, China, 2017–2023

Zhibo Xie[1]; Zhen Zhu[1]; Jin Xu[2]; Naiying Mao[1]; Aili Cui[1]; Wenhui Wang[2]; Yage Wang[1]; Zhibo Zhang[3];
Baicheng Xia[1]; Haoran Wang[4]; Zhen Sun[4]; Yan Zhang[1,#]

ABSTRACT

Introduction: This study examines the seasonal and genetic characteristics of human metapneumovirus (HMPV) in Henan from 2017 to 2023.

Methods: Samples from patients with acute respiratory infection (ARI) testing positive for HMPV were subjected to real-time reverse transcription polymerase chain reaction The G gene was amplified and sequenced from these samples for epidemiological and phylogenetic analysis.

Results: We enrolled 2,707 ARI patients from October 2017 to March 2023, finding an HMPV positivity rate of 6.17% (167/2,707). Children under five exhibited the highest infection rate at 7.78% (138/1,774). The 2018 and 2019 HMPV outbreaks predominantly occurred in spring (March to May), with peak positivity rates of 31.11% in May 2018 and 19.57% in May 2019. A notable increase occurred in November 2020, when positivity reached a historic high of 42.11%, continuing until January 2021. From February 2021 through March 2023, no significant seasonal peaks were observed, with rates ranging from 0% to 8.70%. Out of 81 G gene sequences analyzed, 46.91% (38/81) were identified as subtype A (A2c: 45.67%, 37/81; A2b: 1.23%, 1/81) and 53.09% (43/81) as subtype B (B1: 9.88%, 8/81; B2: 43.21%, 35/81). Notably, an AAABBA switch pattern was observed in HMPV subtypes. The dominant strains were A2c$_{111\text{nt-dup}}$ in subtype A and B2 in subtype B.

Conclusions: Six years of surveillance in Henan Province has detailed the seasonal and genetic dynamics of HMPV, contributing valuable insights for the control and prevention of HMPV infections in China. These findings support the development of targeted HMPV vaccines and immunization strategies.

Human metapneumovirus (HMPV) is a prevalent pathogen responsible for acute respiratory infections (ARIs) across various demographic groups, including children, adults, the elderly, and immunocompromised individuals (*1*). In 2018, it was estimated that around 11.1 million cases of acute lower respiratory infections globally were attributable to HMPV, leading to approximately 502,000 hospitalizations and 113,000 fatalities (*2*). The most frequently observed clinical manifestations of HMPV infection entail infections of both the upper and lower respiratory tracts (*3*).

HMPV is a single-stranded, negative-sense, nonsegmented RNA virus (*4*). In 2016, HMPV was reclassified into the *Metapneumovirus* genus within the family *Pneumoviridae* (*5*). Its genome comprises eight genes that encode nine proteins. F gene and G gene code for the fusion protein (F protein) and the attachment glycoprotein (G protein), respectively, which are primary targets for the molecular typing of HMPV. Based on the antigenic properties of the G or F proteins, HMPV is categorized into subtypes A and B, further divided into six genotypes: A1, A2a, A2b, A2c, B1, and B2 (*6*). Notably, HMPV strains exhibiting 180 and 111 nucleotide duplications (nt-dup) in the G gene have been identified in Japan since 2014 and in Spain since 2017, respectively (*7*–*8*). Phylogenetic analyses have placed these variants within the A2c genotype, designating them as A2c$_{180\text{nt-dup}}$ and A2c$_{111\text{nt-dup}}$ strains. Given that the G gene is the most variable region of the HMPV genome and prone to large nt-dup, it is particularly useful for genotyping efforts. In China, the A2c$_{111\text{nt-dup}}$ strains have been detected in Guangdong, Beijing, and Shandong provinces, suggesting their potential emergence as dominant strains (*9*).

Following the COVID-19 pandemic, global reports have indicated seasonal variations in the epidemiology of influenza virus and human respiratory syncytial virus (HRSV) infections (*10*). In the United States, the early 2023 detection rates for HMPV rose from 7% to between 10% and 19% (*11*). However, the epidemiological understanding and genetic profiling of

HMPV in China remain underexplored, particularly post-COVID-19. Henan, a populous province, has maintained ongoing surveillance for influenza-like illness (ILI) since 2010 and severe acute respiratory infection (SARI) since 2015. These surveillance efforts provide a unique opportunity to examine the prevalence and genetic attributes of HMPV. Consequently, this study leveraged the ILI and SARI surveillance data from Henan to assess the epidemiological and genetic trends of HMPV, aiming to enhance HMPV infection control measures in China and support the development of relevant vaccines and immunization policies.

METHODS

Case Definition and Sources

ILI and SARI cases were recruited from Luohe Central Hospital, a national ILI and SARI surveillance sentinel hospital in Henan, from October 2017 to March 2023. In accordance with WHO guidelines, ILI cases were defined as “an acute respiratory illness with a measured temperature of ≥38 °C and cough, with onset within the last 10 days,” while SARI cases were defined as “an acute respiratory illness with a history of fever or measured fever of ≥38 °C and cough, with onset within the last 10 days that necessitates hospitalization” (*12*). Standardized forms were utilized to gather epidemiological and clinical data from enrolled patients, and throat swab samples were collected for analysis.

HMPV Identification and G Gene Sequencing

After extracting nucleic acids from patients diagnosed with ARI, we carried out viral detection using multiplex real-time reverse transcription polymerase chain reaction (qRT−PCR) (Kinghawk, Beijing, China). This method successfully identified nine viruses, including HMPV (*13*). We then detailed the epidemiological and clinical features of patients who tested positive for HMPV. Subsequently, the full-length G genes of HMPV (ranging from 654 to 867 base pairs) were amplified using RT-PCR, following methodologies previously described (*13*). Amplicons that tested positive were subjected to Sanger sequencing. The sequences were then assembled using Sequencher software version 5.4.5 (GeneCode, Ann Arbor, Michigan, USA) to derive the complete sequences of the HMPV G genes.

Bioinformatics Analysis

The phylogenetic analysis of the HMPV G gene was conducted using MEGA software version 7.0 (Mega Ltd., Auckland, New Zealand) (*14*). This analysis incorporated sequences derived from this study and representative HMPV sequences downloaded from GenBank. The maximum likelihood method was utilized to construct the phylogenetic tree. To test the reliability of tree topologies, bootstrapping with 1000 replicates was performed. Evolutionary distances were calculated using the Kimura 2-parameter method. Additionally, the Chiplot online tool was employed for phylogenetic tree construction (*15*). Genetic distances within and between groups were also computed using MEGA software.

Statistical Analysis

The IBM SPSS software, version 22.0 (IBM Corp., Armonk, N.Y., USA), was employed for statistical analysis. The Chi-square test was utilized to assess the differences in positive rates across various cases, sexes, age groups, and months. Two-tailed p-values less than 0.05 were considered statistically significant.

RESULTS

Clinical Characteristics of HMPV Patients

In this study, a total of 2,707 patients with ARIs were included, consisting of 2,201 with SARIs and 506 with ILIs. Through qRT-PCR analysis, 167 samples (6.17%) tested positive for HMPV. The prevalence of HMPV was higher in patients with ILIs (9.09%, 46/506) compared to those with SARIs (5.50%, 121/2,201) (χ^2=9.177, *P*=0.002). The infection rate was also greater in females (7.24%, 84/1,160) than in males (5.37%, 83/1,547) (χ^2=4.031, *P*=0.045) (Table 1). The age of participants ranged from 5 months to 17 years, with the highest percentage of HMPV positivity (7.78%, 138/1,774) observed in children under 5 years old (χ^2=26.742, *P*<0.001). Among this age group, the lowest positivity rate (3.19%, 6/188) was found in children under 1 year old (χ^2=9.54, *P*=0.049) (Table 1).

Among the HMPV-positive patients, 72.46% (121/167) had single infections, while 27.54% (46/167) were co-infected with one to three other respiratory viruses, such as HRSV (4.79%, 8/167), rhinovirus (4.79%, 8/167), and influenza virus (4.19%, 7/167) (Supplementary Table S1, available at https://weekly.chinacdc.cn/). The predominant clinical

TABLE 1. Characteristics of the population comprising enrolled patients with ARIs and those testing positive for HMPV.

Group	Frequency of enrolled patients (*n*=2,707)	Frequency of HMPV-positive patients (%) (*n*=167)	χ^2	*P* value
Case group			9.177	0.002
ILI	506	46 (9.09)		
SARI	2,201	121 (5.05)		
Sex			4.031	0.045
Male	1,547	83 (5.37)		
Female	1,160	84 (7.24)		
Age group			26.742	<0.001
0–4 years	1,774	138 (7.78)*		
5–17 years	634	26 (4.15)		
17–59 years	173	1 (0.58)		
60–96 years	134	2 (1.49)		
Age (<5 years old)			9.540	0.049
<1 year	188	6 (3.19)†		
1 year	634	54 (8.52)		
2 years	278	16 (5.76)		
3 years	433	39 (9.01)		
4 years	241	23 (9.54)		

Abbreviation: HMPV=human metapneumovirus; ILI=influenza-like illness; SARI=severe acute respiratory infection.

* Pairwise comparisons across various age groups revealed that the highest HMPV positivity rate was observed in children aged 0 to 4 years.

† Among children under 5 years old, pairwise comparisons indicated that the HMPV positivity rate was lowest in children younger than 1 year.

symptoms included fever (42.51%, 71/167), cough (41.32%, 69/167), and expectoration (14.37%, 24/167). Furthermore, 50.90% (85/167) of the HMPV-positive patients were diagnosed with pneumonia, and 9.59% (16/167) with bronchitis. Patients with only HMPV infection exhibited a lower incidence of fever (χ^2=5.901, *P*=0.015) and cough (χ^2=7.908, *P*=0.005) compared to those with co-infections (Supplementary Table S2, available at https://weekly.chinacdc.cn/).

Temporal Distribution of HMPV Infection

During the 2018–2019 period, the typical HMPV outbreak season was identified as spring, spanning from March to May (Figure 1). The peak incidence rates for these years were recorded in May, with 31.11% (14/45) in 2018 and 19.57% (9/46) in 2019. However, the pattern shifted significantly beginning in 2020. An atypical surge in HMPV cases occurred from November 2020 to January 2021, peaking in November 2020 with a positivity rate of 42.11% (32/76) (Figure 1). In contrast, HMPV was undetectable from April to December 2021. Furthermore, from January 2022 through March 2023, the HMPV positivity rate remained low, ranging from 0% to 8.11%, and did not exhibit any distinct seasonal peak.

Genetic Characteristics of HMPV

Using HMPV-specific RT-PCR and Sanger sequencing, we successfully extracted 81 G gene sequences of HMPV from 167 HMPV-positive samples. Phylogenetic analysis (Figure 2) revealed that 46.91% (38/81) of these sequences corresponded to subtype HMPV-A, while 53.09% (43/81) were classified as HMPV-B.

According to the phylogenetic analysis, the sequences identified in this study were categorized into four genotypes: A2c (45.67%, 37/81), A2b (1.23%, 1/81), B1 (9.88%, 8/81), and B2 (43.21%, 35/81). Within each genotype, the sequences displayed high homology, exhibiting nucleotide identities ranging from 90.48% to 100%.

Among the A2c strains, 94.59% (35 out of 37) sequences exhibited nucleotide duplications (nt-dup) in the G gene. These were categorized into A2c$_{\text{180nt-dup}}$ (17.14%, 6 out of 35) and A2c$_{\text{111nt-dup}}$ (82.86%, 29 out of 35) variants. Nucleotide identity within the

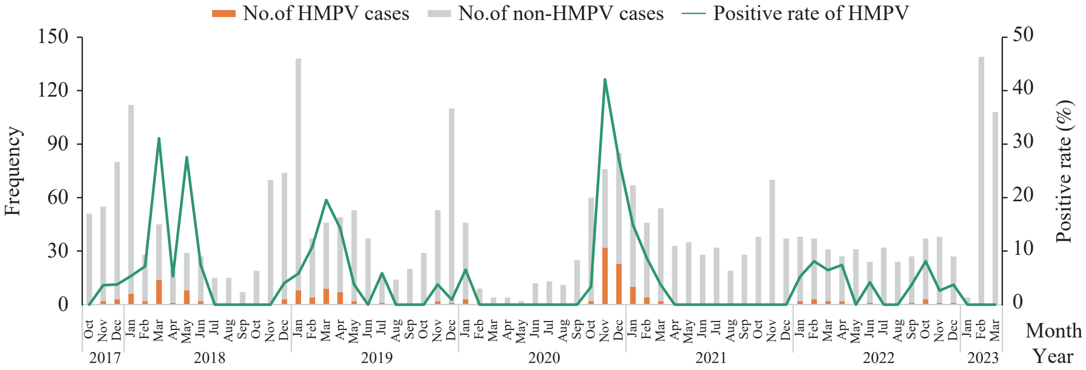

FIGURE 1. Temporal distribution of HMPV cases in Henan Province, China.
Note: "No." represents the number of cases.
Abbreviation: HMPV=human metapneumovirus.

A2c$_{111\text{nt-dup}}$ sequences ranged from 92.61% to 100%, while it spanned from 99.07% to 100% among the A2c$_{180\text{nt-dup}}$ variants.

Circulation Patterns of HMPV Subtypes and Genotypes

HMPV-A represented a significant proportion of cases in 2017 (100%, 1/1), 2018 (80%, 16/20), 2019 (70%, 14/20), and 2022 (87.5%, 7/8). Conversely, HMPV-B dominated in 2020 (100%, 23/23) and 2021 (100%, 9/9) (Figure 3A). These findings suggest that either HMPV-A or HMPV-B, or both, were prevalent in different years, exhibiting a possible subtype switching pattern "AAABBA" from 2017 to 2022 in Henan Province (Figure 3A).

In addition to subtype variations, the genotypes of HMPV also fluctuated over the years (Figure 3B). Two A2c strains, lacking both the 111nt-dup and 180nt-dup variations, were identified exclusively in 2018. Meanwhile, the A2c$_{180\text{nt-dup}}$ variant was observed during 2017–2018. The A2c$_{111\text{nt-dup}}$ variant was first identified in 2018 and subsequently emerged as the prevalent strain of HMPV-A in Henan during 2019 and 2022. The B2 genotype became the predominant strain of HMPV-B in 2020 and 2022 (Figure 3B).

DISCUSSION

To better understand the seasonal and genetic characteristics of HMPV, a retrospective study was carried out in Henan, China, from October 2017 to March 2023. The overall positivity rate for HMPV was 6.17%. The majority of HMPV cases occurred in children under five years of age, aligning with previously documented age distributions and positivity rates (*16*). Among children younger than five, the lowest positivity rate for HMPV was observed in infants under one year of age. However, previous research indicates that this age group exhibits the highest positivity rate for HRSV (*17*). Consequently, the demographic most susceptible to HMPV appears to be slightly older than that for HRSV.

In the Northern Hemisphere, HMPV typically reaches its peak prevalence during the winter and spring months. Similarly, in China, the highest incidence of HMPV occurs from March to May (*18*). However, this study documents an atypical surge of HMPV during the autumn and winter seasons, with the positivity rate escalating to an unprecedented 42.11% in November 2020, compared to previous peaks of 31.11% in May 2018 and 19.57% in May 2019. Similar deviations in HMPV activity and seasonal patterns have been observed in various countries (*19*–*21*). For instance, following an initial decline in cases after the COVID-19 outbreak in 2020, South Korea experienced an off-season epidemic in the autumn of 2022, where HMPV prevalence increased by 2.5 times (*19*). The COVID-19 pandemic led to reduced exposure and transmission of HMPV, weaker maternal antibodies, and subsequently an increased pool of susceptible individuals, potentially contributing to higher than usual HMPV infection rates following the easing of nonpharmaceutical interventions (NPIs). More serological research is essential to determine the underlying factors for these shifts in HMPV prevalence. Additionally, the incidence of ARIs caused by various pathogens, including Mycoplasma pneumoniae, influenza, and HRSV, has also risen in China during the autumn and winter of 2023 (*22*). Continued surveillance of HMPV is critical to further understand these seasonal changes and their

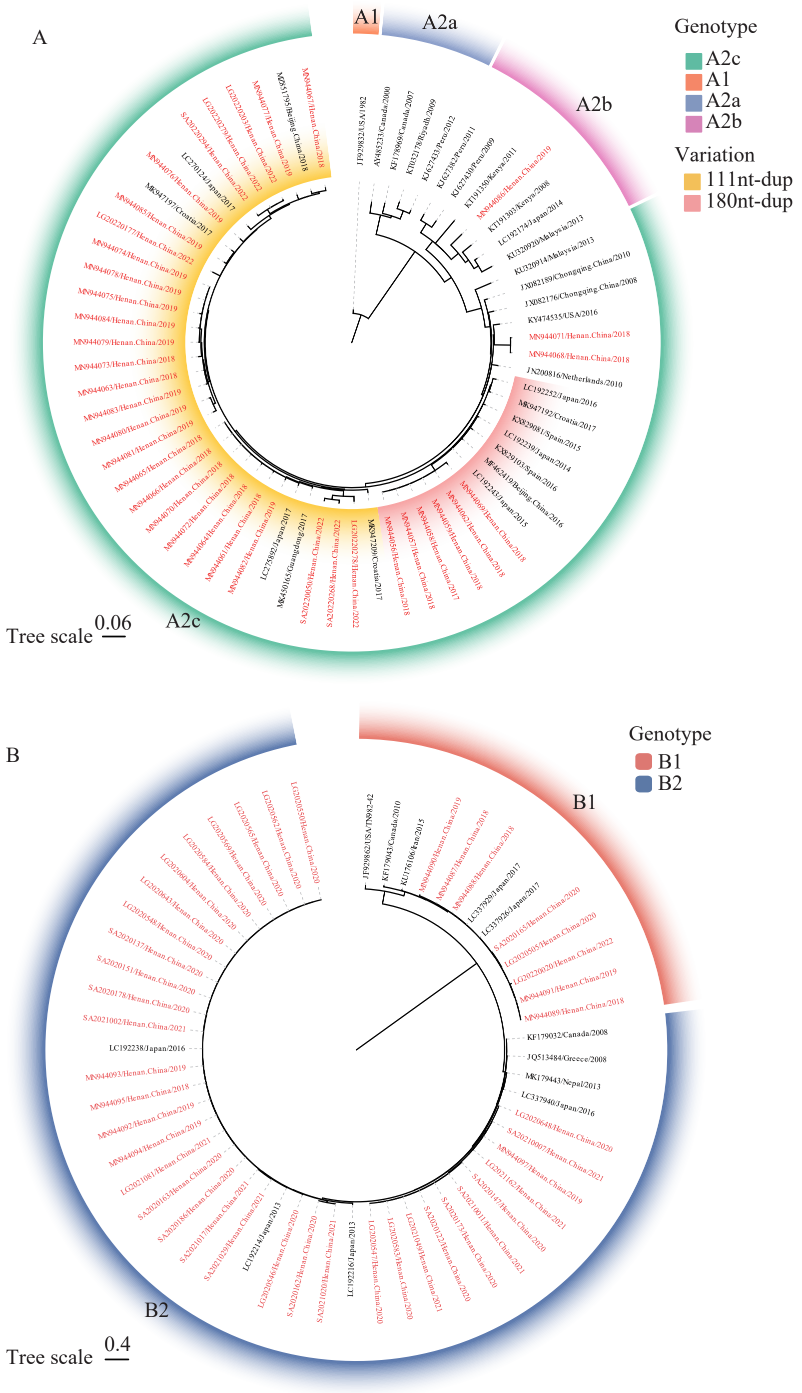

FIGURE 2. The phylogenetic tree of the HMPV G gene for (A) subtype A and (B) subtype B, constructed using the maximum likelihood method.
Note: Sequences from this study are highlighted in red, and the representative strains are shown in white.
Abbreviation: nt-dup=nucleotide duplication; HMPV=human metapneumovirus.

implications in China.

Genetic analysis from this study suggests that HMPV-A and HMPV-B either prevailed independently or concurrently over different years, displaying a potential subtype switch pattern described as "AAABBA" from 2017 to 2022 in Henan Province. A comparable switching pattern has been observed in HRSV (*23*). However, these findings could be impacted by sampling bias and the relatively low rate of sequence recovery from positive samples (48.50%). Additional data is needed to further investigate the subtype switching patterns and genotype evolution in

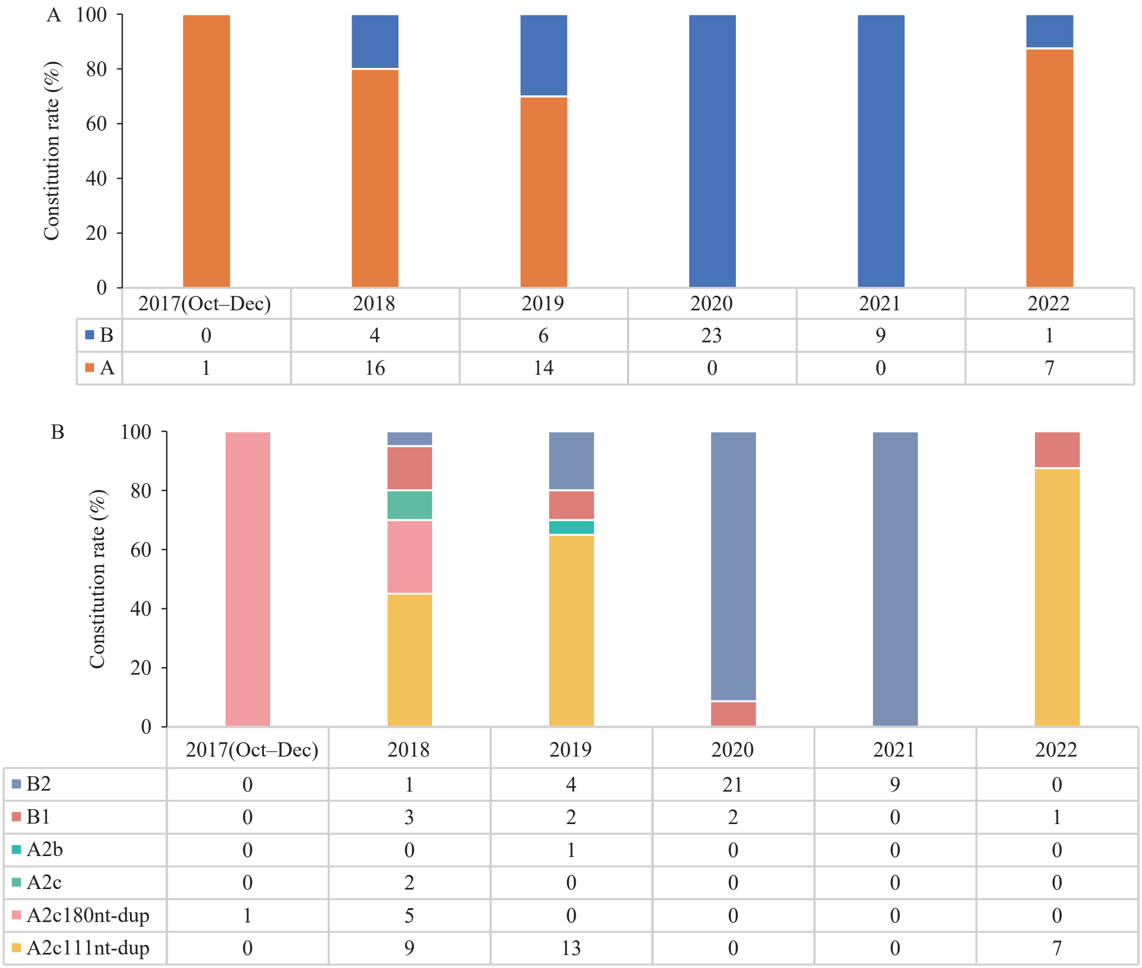

	2017(Oct–Dec)	2018	2019	2020	2021	2022
■ B	0	4	6	23	9	1
■ A	1	16	14	0	0	7

	2017(Oct–Dec)	2018	2019	2020	2021	2022
■ B2	0	1	4	21	9	0
■ B1	0	3	2	2	0	1
■ A2b	0	0	1	0	0	0
■ A2c	0	2	0	0	0	0
■ A2c180nt-dup	1	5	0	0	0	0
■ A2c111nt-dup	0	9	13	0	0	7

FIGURE 3. Proportions of HMPV (A) subtypes and (B) genotypes circulating in Henan Province, China, across various years.
Note: The accompanying table presents the count of sequences for each subtype or genotype.
Abbreviation: A2c=strains lacking duplications of 111 or 180 nucleotides in the G gene; nt-dup=nucleotide duplication.

HMPV.

In this study, 94.59% (35/37) of the A2c strains were classified into two variants: A2c$_{\text{180nt-dup}}$, forming 17.14% (6/35), and A2c$_{\text{111nt-dup}}$, comprising 82.86% (29/35). Initially identified in 2014 and 2017, respectively, these strains have emerged as the predominant HMPV-A strains worldwide during the period 2016–2021 (*24*–*25*). Surveillance data from six sentinel hospitals in China, collected between 2017 and 2019, indicated that the A2c$_{\text{111nt-dup}}$ variant represented 44.44% (16/36) of HMPV-A cases (*16*). This study expands on these findings by providing genetic insights from ongoing surveillance of HMPV in Henan over the past six years. It was observed that the A2c$_{\text{111nt-dup}}$ became the dominant strain in 2019 and maintained this status until 2022. Notably, the substantial duplication in the dominant A2c$_{\text{111nt-dup}}$ variants augmented potential glycosylation sites and extended the extracellular domain of the G protein (*13*,*26*). The implications of these modifications on the functionality of the HMPV G protein warrant further investigation.

This study is subject to some limitations. First, the rigorous enforcement of NPIs during the early phase of the COVID-19 pandemic resulted in a lower enrollment of patients with ARIs, potentially skewing the analysis of their temporal distribution. Second, it was challenging to determine changes in the seasonal patterns of HMPV due to potential influences from various factors. These factors include changes in immune reserve capacities prompted by NPIs and interactions with other respiratory viruses. Additionally, since only 48.50% (81/167) of HMPV-positive cases had G gene sequences available, the conclusions regarding shifts in HMPV subtypes and genotypes might be subject to bias.

In conclusion, this study has presented six years of consecutive surveillance data on HMPV in Henan, China, elucidating the epidemic patterns and genetic characteristics of the virus. This information could inform strategies for the prevention and control of HMPV infection in China and aid in the development of vaccines and immunization tactics.

Conflicts of interest: No conflicts of interest.

Funding: Supported by the National Health Commission Major Public Health Project (ZDGWXFTF23-04).

doi: 10.46234/ccdcw2024.087

[#] Corresponding author: Yan Zhang, zhangyan@ivdc.chinacdc.cn.

---

[1] National Key Laboratory of Intelligent Tracking and Forecasting for Infectious Diseases, NHC Key Laboratory of Medical Virology and Viral Disease, National Institute for Viral Disease Control and Prevention, Chinese Center for Disease Control and Prevention, Beijing, China; [2] Henan Provincial Center for Disease Control and Prevention, Luohe City, Henan Province, China; [3] Luohe Center for Disease Control and Prevention, Luohe City, Henan Province, China; [4] Luohe Central Hospital, Luohe City, Henan Province, China.

Submitted: April 08, 2024; Accepted: May 11, 2024

REFERENCES

1. Esposito S, Mastrolia MV. Metapneumovirus infections and respiratory complications. Semin Respir Crit Care Med 2016;37(4):512 – 21. https://doi.org/10.1055/s-0036-1584800.
2. Wang X, Li Y, Deloria-Knoll M, Madhi SA, Cohen C, Ali A, et al. Global burden of acute lower respiratory infection associated with human metapneumovirus in children under 5 years in 2018: a systematic review and modelling study. Lancet Glob Health 2021;9(1): e33 – 43. https://doi.org/10.1016/S2214-109X(20)30393-4.
3. Howard LM, Edwards KM, Zhu YW, Griffin MR, Weinberg GA, Szilagyi PG, et al. Clinical features of human metapneumovirus infection in ambulatory children aged 5-13 Years. J Pediatric Infect Dis Soc 2018;7(2):165 – 8. https://doi.org/10.1093/jpids/pix012.
4. van den Hoogen BG, de Jong JC, Groen J, Kuiken T, de Groot R, Fouchier RAM, et al. A newly discovered human pneumovirus isolated from young children with respiratory tract disease. Nat Med 2001;7(6): 719 – 24. https://doi.org/10.1038/89098.
5. Rima B, Collins P, Easton A, Fouchier R, Kurath G, Lamb RA, et al. ICTV virus taxonomy profile: *Pneumoviridae*. J Gen Virol 2017;98(12): 2912 – 3. https://doi.org/10.1099/jgv.0.000959.
6. Yi LN, Zou LR, Peng JJ, Yu JX, Song YC, Liang LJ, et al. Epidemiology, evolution and transmission of human metapneumovirus in Guangzhou China, 2013-2017. Sci Rep 2019;9(1):14022. https://doi.org/10.1038/s41598-019-50340-8.
7. Saikusa M, Nao N, Kawakami C, Usuku S, Sasao T, Toyozawa T, et al. A novel 111-nucleotide duplication in the G gene of human metapneumovirus. Microbiol Immunol 2017;61(11):507 – 12. https://doi.org/10.1111/1348-0421.12543.
8. Piñana M, Vila J, Gimferrer L, Valls M, Andrés C, Codina MG, et al. Novel human metapneumovirus with a 180-nucleotide duplication in the *G* gene. Future Microbiol 2017;12(7):565 – 71. https://doi.org/10.2217/fmb-2016-0211.
9. Liu ZR, Xie ZB, Sun R, Zhang F, Xu WB, Wang ZG, et al. The $A2c_{111nt\text{-}dup}$ variants of human metapneumovirus predominantly circulating in Qingdao, China, during 2018 and 2019. J Med Virol 2022;94(9):4301 – 8. https://doi.org/10.1002/jmv.27888.
10. Agca H, Akalin H, Saglik I, Hacimustafaoglu M, Celebi S, Ener B. Changing epidemiology of influenza and other respiratory viruses in the first year of COVID-19 pandemic. J Infect Public Health 2021;14(9): 1186 – 90. https://doi.org/10.1016/j.jiph.2021.08.004.
11. Centers for Disease Control and Prevention. National respiratory and enteric virus surveillance system. 2024. https://www.cdc.gov/surveillance/nrevss/index.html#:~:text=The%20National%20Respiratory%20and%20Enteric%20Virus%20Surveillance%20System,%28HMPV%29%2C%20respiratory%20adenoviruses%2C%20human%20coronavirus%2C%20rotavirus%2C%20and%20norovirus. [2024-3-15].
12. Fitzner J, Qasmieh S, Mounts AW, Alexander B, Besselaar T, Briand S, et al. Revision of clinical case definitions: influenza-like illness and severe acute respiratory infection. Bull World Health Organ 2018;96(2):122 – 8. https://doi.org/10.2471/BLT.17.194514.
13. Xie ZB, Xu J, Ren YH, Cui AL, Wang HL, Song JH, et al. Emerging human metapneumovirus gene duplication variants in patients with severe acute respiratory infection, China, 2017-2019. Emerg Infect Dis 2021;27(1):275 – 7. https://doi.org/10.3201/eid2701.201043.
14. Kumar S, Stecher G, Tamura K. MEGA7: molecular evolutionary genetics analysis version 7. 0 for bigger datasets. Mol Biol Evol 2016;33(7):1870 – 4. https://doi.org/10.1093/molbev/msw054.
15. Xie JM, Chen YR, Cai GJ, Cai RL, Hu Z, Wang H. Tree Visualization By One Table (tvBOT): a web application for visualizing, modifying and annotating phylogenetic trees. Nucleic Acids Res 2023;51(W1): W587 – 92. https://doi.org/10.1093/nar/gkad359.
16. Zhao HW, Feng QY, Feng ZH, Zhu Y, Ai JH, Xu BP, et al. Clinical characteristics and molecular epidemiology of human metapneumovirus in children with acute lower respiratory tract infections in China, 2017 to 2019: A multicentre prospective observational study. Virol Sin 2022;37(6):874 – 82. https://doi.org/10.1016/j.virs.2022.08.007.
17. Cui AL, Xie ZB, Xu J, Hu KX, Zhu RN, Li Z, et al. Comparative analysis of the clinical and epidemiological characteristics of human influenza virus versus human respiratory syncytial virus versus human metapneumovirus infection in nine provinces of China during 2009–2021. J Med Virol 2022;94(12):5894 – 903. https://doi.org/10.1002/jmv.28073.
18. Wei TL, Wang C, Ma FL, Guo JQ, Chen AJ, Huang YM, et al. Whole genome sequencing and evolution analyses of *Human metapneumovirus*. Virus Genes 2023;59(4):524 – 31. https://doi.org/10.1007/s11262-023-02001-2.
19. Cho SJ, Kim SH, Lee H, Lee YU, Mun J, Park S, et al. Re-emergence of HMPV in Gwangju, South Korea, after the COVID-19 pandemic. Pathogens 2023;12(10):1218. https://doi.org/10.3390/pathogens12101218.
20. Piñana M, González-Sánchez A, Andrés C, Abanto M, Vila J, Esperalba J, et al. The emergence, impact, and evolution of human metapneumovirus variants from 2014 to 2021 in Spain. J Infect 2023;87(2):103 – 10. https://doi.org/10.1016/j.jinf.2023.05.004.
21. Farfour É, Rouabah L, Bargain P, Lecuru M, Picard C, Tcherakian C, et al. Trend in respiratory viruses' activity in the COVID-19 area. Ann Biol Clin (Paris) 2023;81(4):403 – 9. https://doi.org/10.1684/abc.2023.1827.
22. World Health Organization. Upsurge of respiratory illnesses among children-Northern China. 2023. https://www.who.int/emergencies/disease-outbreak-news/item/2023-DON494. [2024-3-15].
23. Song JJ, Zhu Z, Song JH, Mao NY, Cui AL, Xu WB, et al. Circulation pattern and genetic variation of human respiratory syncytial virus in China during 2008-2021. J Med Virol 2023;95(3):e28611. https://doi.org/10.1002/jmv.28611.
24. Parida P, N S, E R S, Jagadesh A, Marate S, Govindakaranavar A. The emergence of human metapneumovirus G gene duplication in hospitalized patients with respiratory tract infection, India, 2016–2018. Mol Biol Rep 2023;50(2):1109-16. http://dx.doi.org/10.1007/s11033-022-08092-8.
25. Groen K, van Nieuwkoop S, Meijer A, van der Veer B, van Kampen JJA, Fraaij PL, et al. Emergence and potential extinction of genetic lineages of human metapneumovirus between 2005 and 2021. mBio 2023;14(1):e02280 – 22. https://doi.org/10.1128/mbio.02280-22.
26. Piñana M, Vila J, Maldonado C, Galano-Frutos JJ, Valls M, Sancho J, et al. Insights into immune evasion of human metapneumovirus: novel 180- and 111-nucleotide duplications within viral G gene throughout 2014-2017 seasons in Barcelona, Spain. J Clin Virol 2020;132:104590. https://doi.org/10.1016/j.jcv.2020.104590.

SUPPLEMENTARY MATERIAL

SUPPLEMENTARY TABLE S1. The simple or co-infected viruses detected in the HMPV positive cases.

Viral pathogen	Number of cases (%)
Simple infection of HMPV	121 (72.46)
Co-infected with two viruses	41 (24.55)
HMPV+HRSV	7 (4.19)
HMPV+RV	7 (4.19)
HMPV+IFV	6 (3.59)
HMPV+HBoV	6 (3.59)
HMPV+EV	5 (2.99)
HMPV+HAdV	4 (2.40)
HMPV+HCoV	4 (2.40)
HMPV+HPIV	2 (1.20)
Co-infected with three viruses	4 (2.40)
HMPV+HCoV+HAdV	1 (0.60)
HMPV+IFV+HPIV	1 (0.60)
HMPV+HPIV+EV	1 (0.60)
HMPV+HRSV+HPIV	1 (0.60)
Co-infected with four viruses	1 (0.60)
HMPV+RV+HPIV+HCoV	1 (0.60)
Total	167 (100.00)

Abbreviation: HMPV=human metapneumovirus; HRSV=human respiratory syncytial virus; RV=rhinovirus; IFV=influenza virus; HBoV=human bocavirus; EV=enterovirus; HAdV=human adenovirus; HCoV= human coronavirus; HPIV=human parainfluenza virus.

SUPPLEMENTARY TABLE S2. The clinical symptoms and diagnosis of simple or co-infection cases of HMPV.

Symptoms or diagnosis	Simple infection of HMPV (*n*=121)	Co-infection with HMPV (*n*=46)	χ^2	*P*	Total of HMPV positive cases (*n*=167)
Symptoms					
Fever	44 (36.36)	27 (58.70)	5.901	0.015	71 (42.51)
Cough	42 (34.71)	27 (58.70)	7.908	0.005	69 (41.32)
Expectoration	17 (14.05)	7 (15.22)	0.037	0.848	24 (14.37)
Running nose	7 (5.79)	1 (2.17)	0.326	0.568	8 (4.79)
Sore throat	1 (0.83)	3 (6.52)	2.509	0.113	4 (2.40)
Diagnosis					
Pneumonia	59 (48.76)	26 (56.52)	0.803	0.370	85 (50.90)
Bronchitis	9 (7.44)	7 (15.22)	1.517	0.218	16 (9.58)

Abbreviation: HMPV=human metapneumovirus.

Vital Surveillances

Epidemiological Characterization of Dengue Fever — Yunnan Province, China, 2010–2021

Xiaoxiang Zhu[1]; Songwang Wang[1]; Yanfei Li[1]; Yu Cao[1]; Xuemei Su[1,#]; Xiaotao Zhao[2,#]

ABSTRACT

Objective: The goal of this study is to analyze the epidemiological patterns of dengue fever across different districts and counties in Yunnan Province from 2010 to 2021.

Methods: In this study, we employed joinpoint regression analysis, spatial autocorrelation analysis, and space-time scan analysis to illustrate the spatio-temporal propagation and demographic influence of dengue fever, using both graphical and tabular presentations to clearly demonstrate the findings.

Results: Yunnan Province reported 14,098 cases of dengue fever during the period from 2010 to 2021. Of these, 11,513 cases were caused by local transmission, 2,566 were imported internationally, and 19 were inter-provincial imports. Seasonal trends emerged, revealing a surge in incidences during the summer and autumn months. The sex ratio of male to female cases was 1:0.88, with a significant majority of 82.00% of cases involving individuals belonging to the age group of 15–60. Commercial service workers constituted the most impacted occupational group, forming 20.96% of total cases. A spatio-temporal scan identified significant clustering of dengue fever cases across space and time, with the most pronounced cluster observed in southern Yunnan, primarily between 2015 and 2019.

Conclusions: Dengue fever in Yunnan Province manifests as biennial outbreaks, underscoring the necessity for increased surveillance, particularly in counties bordering other regions.

Dengue fever, a mosquito-borne illness, can be caused by any of the four dengue virus serotypes (*1*). Currently, over 100 tropical and subtropical countries are disease-endemic, thus exposing more than a third of the global population to the risk of infection (*2*). Since 1978, there have been significant outbreaks in Chinese mainland, resulting in 655,324 confirmed cases and 610 deaths until 2008. Initially, clustering was observed in southern coastal provincial-level administrative divisions (PLADs) like Guangdong, Hainan, and Guangxi. Nevertheless, the disease distribution started extending northward and westward to include PLADs such as Fujian, Zhejiang, and Yunnan in the 1990s (*3*–*4*). Yunnan encountered its first imported case in 1975 but, notably, no other cases were reported for the ensuing 25 years. Despite the sporadic importations of the disease between 2000 and 2007, a significant shift occurred in 2008 when twelve indigenous cases emerged in five border areas of Zhenkang, Mangshi, Yingjiang, Ruili, and Longchuan, indicating the first occurrence of local transmission in the PLAD. An increasing trend in local dengue outbreaks has been noticed recently, both in terms of frequency and geographical distribution since 2010 (*5*–*6*). Thus, this paper seeks to elucidate the changing epidemiological characteristics of dengue fever in Yunnan from 2010 to 2021 by examining three distinct periods of the disease's outbreaks within the PLAD.

METHODS

This research utilized dengue case data from the China Disease Control and Prevention Information System (CDCIS) covering the period from 2010 to 2021. This encompassed both laboratory-confirmed and clinically-diagnosed cases, based on the Diagnostic Criteria for dengue fever (WS 216-2008). The data captured detailed information including patient demographics, inception date of symptoms, diagnostic method, and for cases contracted internationally, a travel history to dengue-endemic regions within a fortnight preceding the onset of symptoms.

The data were analyzed using R statistical software (version 4.3.1, R Foundation for Statistical Computing, Auckland, New Zealand) for case information organization. Microsoft Excel 2016

(Microsoft, Redmond, USA) was utilized for demographic analysis. Joinpoint statistical software (version 5.0.2, Applications Branch, National Cancer Institute, Bethesda, USA) was used to investigate trends in dengue incidence rates and stage characteristics over the study period. The spatio-temporal spread of dengue fever was visually represented using ArcMap (version 10.7, Environmental Systems Research Institute, RedLands, USA) and SaTScan (version 10.1.3, Information Management Services, Maryland, USA). The statistical test significance level was set at 0.05.

RESULTS

Epidemic Overview

From 2010 to 2021, Yunnan Province reported 14,098 cases of dengue infection. Of these, 11,513 were locally transmitted, 2,566 were imported from abroad, and 19 were introduced from other PLADs within China. Upon analyzing the infection trends throughout these years, a pattern of sporadic surges was noted. The years 2013, 2015, 2017, and 2019 saw notably high case counts — 1,538, 1,816, 2,575, and 6,471, respectively. Furthermore, from 2013 to 2019, the regions of Xishuangbanna, Dehong, and Lincang experienced dengue outbreaks in a biennial pattern.

A demographic analysis of dengue cases in Yunnan Province reveals a male-to-female case ratio of roughly 1:0.88. Case ages span from one month to 94 years old, with the majority of cases (approximately 79.83%) identified in adults aged 15–59 years. Cases in children aged 0–14 years constitute about 7.65% of the total, with seniors aged 60 years and above comprising 12.52%. Commercial service workers (2,955 cases), farmers (2,888 cases), and either unemployed individuals or domestic workers (1,569 cases) were identified as the most affected occupational groups, accounting for 20.96%, 20.49%, and 11.13% of total cases, respectively. Statistical analysis reveals significant yearly variations in the distribution of cases by gender, age, and occupation, as comprehensively detailed in Table 1.

Temporal Distribution

The annual analysis of dengue case numbers across various districts of Yunnan from 2010 to 2021 has revealed a seasonal pattern, with relatively stable, and fewer cases observed during the first half of each year (2.16%). Throughout this period, imported cases were

TABLE 1. Demographic distribution of dengue fever cases in Yunnan Province, 2010–2021.

Item	2010, *n* (%)	2011, *n* (%)	2012, *n* (%)	2013, *n* (%)	2014, *n* (%)	2015, *n* (%)	2016, *n* (%)	2017, *n* (%)	2018, *n* (%)	2019, *n* (%)	2020, *n* (%)	2021, *n* (%)	Total, *n* (%)	*P*
Gender														<0.05*
Male	10 (0.13)	12 (0.16)	18 (0.24)	731 (9.73)	136 (1.81)	927 (12.34)	191 (2.54)	1,298 (17.28)	409 (5.44)	3,618 (48.16)	151 (2.01)	11 (0.15)	7,512 (53.28)	
Female	8 (0.12)	1 (0.02)	6 (0.09)	807 (12.25)	77 (1.17)	889 (13.50)	134 (2.03)	1,277 (19.39)	433 (6.57)	2,853 (43.32)	99 (1.50)	2 (0.03)	6,586 (46.72)	
Age														<0.05*
0–14	0 (0.00)	1 (0.09)	1 (0.09)	114 (10.58)	17 (1.58)	95 (8.81)	32 (2.97)	241 (22.36)	73 (6.77)	482 (44.71)	20 (1.86)	2 (0.19)	1,078 (7.65)	
15–59	17 (0.15)	12 (0.11)	22 (0.20)	1,257 (11.17)	189 (1.68)	1,529 (13.59)	269 (2.39)	2,122 (18.85)	681 (6.05)	4,937 (43.86)	209 (1.86)	11 (0.10)	11,255 (79.83)	
≥60	1 (0.06)	0 (0.00)	1 (0.06)	167 (9.46)	7 (0.40)	192 (10.88)	24 (1.36)	212 (12.01)	88 (4.99)	1,052 (59.60)	21 (1.19)	0 (0.00)	1,765 (12.52)	
Occupation														<0.05*
Commercial service	3 (0.10)	2 (0.07)	7 (0.24)	367 (12.42)	89 (3.01)	429 (14.52)	136 (4.60)	618 (20.91)	197 (6.67)	1,060 (35.87)	44 (1.49)	3 (0.10)	2,955 (20.96)	
Farmer	1 (0.03)	2 (0.07)	4 (0.14)	118 (4.09)	29 (1.00)	347 (12.02)	41 (1.42)	585 (20.26)	134 (4.64)	1,591 (55.09)	34 (1.18)	2 (0.07)	2,888 (20.49)	
Domestic helper	0 (0.00)	0 (0.00)	1 (0.06)	194 (12.36)	13 (0.83)	198 (12.62)	30 (1.91)	294 (18.74)	111 (7.07)	702 (44.74)	25 (1.59)	1 (0.06)	1,569 (11.13)	
Retiree	1 (0.08)	0 (0.00)	0 (0.00)	175 (13.90)	2 (0.16)	135 (10.72)	19 (1.51)	140 (11.12)	96 (7.63)	684 (54.33)	7 (0.56)	0 (0.00)	1,259 (8.93)	
Student	2 (0.19)	2 (0.19)	1 (0.10)	140 (13.58)	17 (1.65)	117 (11.35)	28 (2.72)	212 (20.56)	65 (6.30)	423 (41.03)	23 (2.23)	1 (0.10)	1,031 (7.31)	
Others	11 (0.25)	7 (0.16)	11 (0.25)	544 (12.37)	63 (1.43)	590 (13.42)	71 (1.62)	726 (16.52)	239 (5.44)	2,011 (45.75)	117 (2.66)	6 (0.14)	4,396 (31.18)	
Total	18 (0.13)	13 (0.09)	24 (0.17)	1,538 (10.91)	213 (1.51)	1,816 (12.88)	325 (2.31)	2,575 (18.27)	842 (5.97)	6,471 (45.90)	250 (1.77)	13 (0.09)	14,098	

*: pass Fisher's exact test.

annually recorded, while there was a notable increase in indigenous cases beginning in 2013. Fundamentally, this twelve-year span can be classified into three phases: the early phase (2010–2012), characterized by sporadic and primarily imported cases; the middle phase (2013–2019), which displayed a consistent growth in imported cases alongside a dramatic surge in indigenous cases, with outbreaks occurring biennially; and the last phase (2020–2021), during which both imported and indigenous cases diminished (Figure 1).

The Joinpoint Regression Program analysis discerned a notable alteration in the trend of dengue fever cases in Yunnan Province in 2019 ($P<0.05$). Over the period 2010 to 2019, there was a substantial surge in dengue cases, yielding an annual percentage change (APC) of 85.25% ($P<0.05$). Contrarily, between 2019 and 2021, a precipitous decline in cases was observed, marked by an APC of −95.12% ($P<0.05$) (Figure 2).

The occurrence of dengue fever in Yunnan Province predominantly coincides with the summer and autumn seasons, particularly the latter months of fall. Conversely, the incidence rates during spring and winter are considerably lower, thereby contributing minimally to the annual case count. Monthly analysis indicates a progressive increase in cases starting from June and July each year, culminating in a peak from August to October, followed by a subsequent decline beginning in November. It's worth noting that the resurgence of imported cases precedes that of indigenous cases, yet the latter surge at a quicker pace and peak earlier, as depicted in Figure 3.

Spatial Distribution

Between 2010 and 2021, a total of 14,098 cases of dengue fever were documented in Yunnan Province. Out of the sixteen cities and prefectures in the PLAD, Xishuangbanna, Dehong, and Lincang were most impacted. These locations accounted for 8,640 (61.29%), 3,567 (25.30%), and 1,149 (8.15%) cases, respectively. Considerable cases were also reported in Kunming and Honghe, which accounted for 302 (2.14%) and 136 (0.96%) cases, respectively. Dengue fever was reported annually in Kunming and every year, except in 2010, in Dehong, whilst Xishuangbanna reported cases each year except 2021. Dengue fever cases were less prevalent in Baoshan, Zhaotong, Pu'er, Qujing, Dali, Chuxiong, Yuxi, Wenshan, Lijiang, and Nujiang, as these locations all reported fewer than 100 cases. Wenshan has reported cases intermittently since 2018, Lijiang during provincial-wide outbreak peak years, and Nujiang reported a single case in 2017. However, no cases of dengue fever have been reported in Diqing. A detailed account of cases can be seen in Supplementary Table S1 (available at https://weekly.chinacdc.cn/).

Between 2010 and 2021, dengue fever was identified in 98 out of 129 districts and counties in Yunnan Province. Of these, 11,513 were indigenous cases spread across 10 districts and counties. Additionally, the PLAD reported 2,566 cases of dengue fever imported from other countries, impacting 96 counties and cities across 15 prefectures. The imported cases primarily originated from Southeast Asian and African countries.

The districts with a significantly high number of indigenous cases were Jinghong (7,571 cases), Ruili (2,620 cases), and Mengla (650 cases), which are all border counties. In terms of imported cases, the top

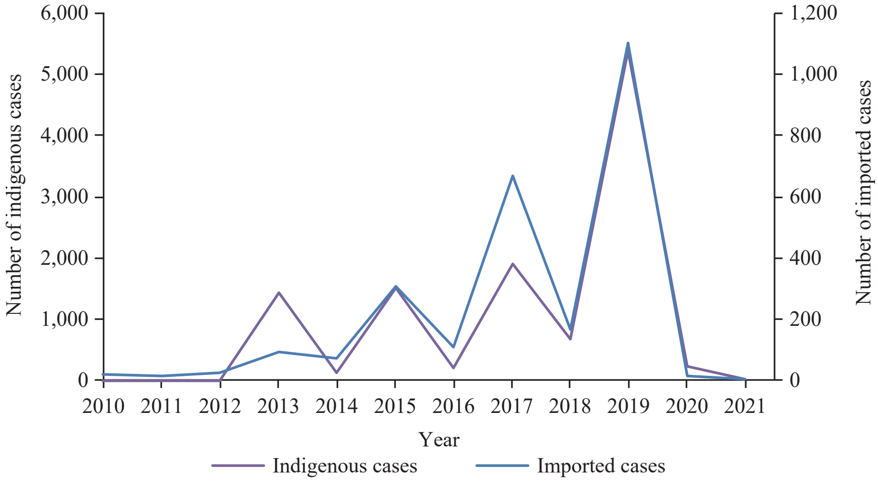

FIGURE 1. Annual distribution of dengue fever cases in Yunnan Province, 2010–2021.

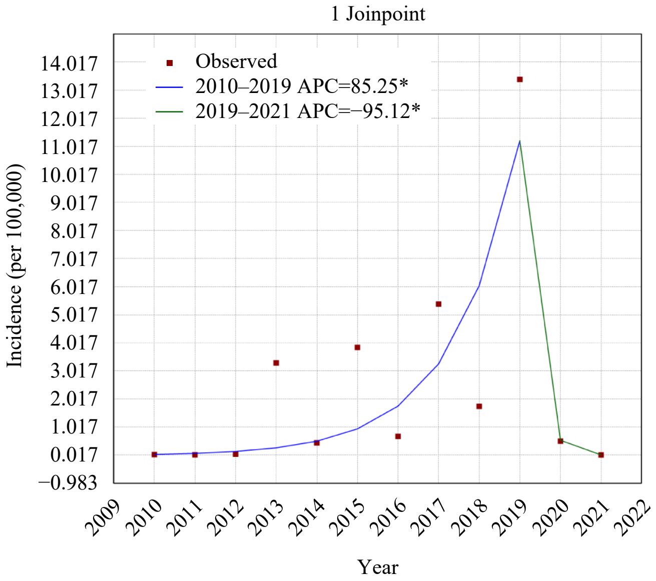

FIGURE 2. Progression of total dengue fever incidence in Yunnan Province, 2010–2021.
Note: Test statistie and *P* value not available for the empirical quantile method. Final selected model: 1 Joinpoint.
Abbreviation: APC=Annual Percent Change.
* Indicates that the Annual Percent Change (APC) is significantly different from zero at the alpha = 0.05 level.

three districts were Ruili (641 cases), Zhenkang (312 cases), and Gengma (299 cases) as outlined in Supplementary Table S2 (available at https://weekly.chinacdc.cn/).

Most of the imported cases were from Southeast Asian countries, accounting for 96.96% of all imported cases. Myanmar reported the highest number of cases (1,937 cases), followed by Cambodia (267 cases), Laos (199 cases), Thailand (62 cases), and Vietnam (23 cases). Both Myanmar and Laos have been regular sources of imported cases since 2010, while Cambodia started reporting cases from 2016 onward.

It is noteworthy to mention that Myanmar reported an increase in the number of cases in 2015, 2017, and 2019. Also, 2019 witnessed an increase in reported cases from Laos and Cambodia as detailed in Supplementary Table S3 (available at https://weekly.chinacdc.cn/).

Furthermore, Yunnan Province recorded 19 cases of dengue fever imported from other PLADs within China, predominantly Guangdong. The majority of these cases were reported in Jinghong, Guandu, and Ruili, with particular spikes in the years 2014 and 2019.

Spatio-Temporal Aggregation

Global spatial autocorrelation analysis: The analysis of global spatial autocorrelation for dengue incidence in Yunnan PLAD suggested significant spatial clustering in specific years. Moran's I values were 0.427 for both 2010 and 2012, followed by 0.05, 0.016, 0.172, 0.107, and 0.128 for 2013, 2016, 2017, 2018, and 2019 correspondingly. These values, with statistical significance ($P<0.05$), indicated considerable spatial clustering of dengue cases. Nevertheless, Moran's I value for 2014 was −0.002 ($P<0.05$), implying a random distribution of cases for that year. During other years, represented by Moran's I values of 0.233, 0.008, and −0.003, the differences were not statistically significant ($P>0.05$), suggesting no noteworthy spatial clustering. Further details can be found in Supplementary Table S4 (available at https://weekly.chinacdc.cn/).

Local spatial autocorrelation analysis: From 2010 to 2021, each year saw the identification of 1 to 5 dengue fever hotspots within the counties of Yunnan PLAD. In the span of 2010 to 2012, these hotspots, largely comprising imported cases, were primarily found in locations such as Jinghong, Ruili, and Kunming. However, between 2013 and 2021, the principal concentration of dengue fever cases transitioned to predominantly include Jinghong and Ruili, with the spread of the disease radiating outward from these two central hotspots. These findings are detailed in Supplementary Table S5 (available at https://weekly.chinacdc.cn/).

Spatio-temporal scan analysis: The spatiotemporal cluster analysis of dengue fever in Yunnan uncovered

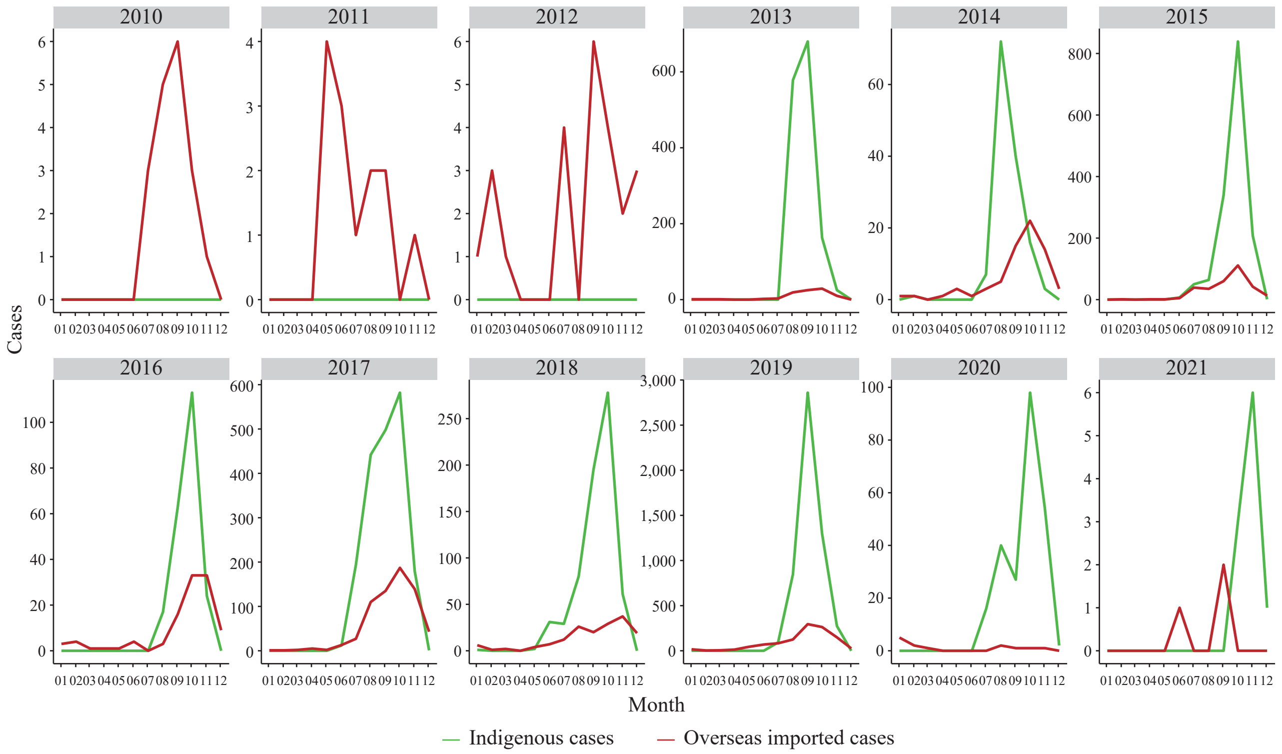

FIGURE 3. Monthly trends in dengue fever cases in Yunnan Province, 2010–2021.

distinctive temporal and spatial patterns. This analysis pinpointed a primary cluster and two secondary clusters via spatial and temporal scan techniques (Supplementary Table S6, available at https://weekly.chinacdc.cn/). The principle cluster was located in the southern quadrant of the PLAD. Its highest-risk phase spanned from 2015 to 2019, marked by a relative risk (RR) of 150.46, a log likelihood ratio (LLR) of 25,770.59, and a highly significant P value ($P<0.001$). This high-risk cluster, which covered a circular area with a radius of 69.29 km and included the counties of Jinghong and Mengla, reported a total of 7,085 dengue fever cases.

CONCLUSIONS

Dengue fever in Yunnan Province is primarily influenced by imported cases, predominantly from Myanmar and Laos, which often result in local outbreaks. This assertion is bolstered by various studies that underscore imported cases as the principal cause of local epidemics, aligning with the results of our research (*7–9*). It is advisable for authorities to diligently observe dengue fever trends in Southeast Asian countries, specifically Myanmar and Laos, during the year's first half. It is imperative to intensify screening procedures at Yunnan's borders, particularly at points of entry.

The border regions of Yunnan have been identified as significant hotspots for transmission, primarily attributed to the Aedes aegypti mosquito (*10*). Over the last decade, the number of affected districts and counties has surged from nine in 2010 to 98 in 2021. This substantial increase may be associated with the widespread presence of the Aedes aegypti mosquito and the mobility of infected individuals (*11–12*). The high density of mosquito populations along the borders, coupled with diverse vector species, coincides with the seasonal spikes of dengue in the PLAD (*13–14*). It is recommended to continue surveillance of the Aedes aegypti mosquito populations, ensure efficient mosquito control, and uphold cleanliness in border areas. Continuous, year-round monitoring is crucial in key regions such as Ruili, Jinghong, and Gengma. Additionally, public health initiatives should drive sanitation practices to prevent the creation of mosquito breeding sites.

There was a discernible alteration in the patterns of dengue occurrence in Yunnan after 2019. This change may be attributed to various factors including the implementation of COVID-19 control measures, enhanced cooperative preventive initiatives, more stringent entry and isolation policies for foreign arrivals, amplified screening and regulation of movement, the endorsement of remote work, the practice of social distancing, and a decline in public mobility (*15*). Collectively, these factors led to a substantial decrease in reported dengue cases.

In conclusion, Yunnan Province has seen sporadic outbreaks of dengue fever, generally on a biennial cycle. Vigilance remains essential regarding the potential increase in prevalence of dengue fever in border counties. Implementing effective dengue surveillance and quarantine measures for travelers originating from regions endemic with to disease is of utmost importance, particularly during large outbreaks or seasons of elevated dengue risk.

Dengue fever in Yunnan Province demonstrates biennial outbreaks, which emphasizes the importance of increased surveillance of the disease in counties located near the border.

Funding: National Science and Technology Infrastructure Platform, National Population and Health Science Data Sharing Service Platform, Public Health Science Data Center (NCMI-ZB01N-201905).

doi: 10.46234/ccdcw2024.088

[#] Corresponding authors: Xuemei Su, suxm@chinacdc.cn; Xiaotao Zhao, zxt_423@163.com.

---

[1] National Key Laboratory of Intelligent Tracking and Forecasting for Infectious Diseases, Chinese Center for Disease Control and Prevention, Beijing, China; [2] Yunnan Institute of Parasitic Diseases, Pu'er City, Yunnan Province, China.

Submitted: January 15, 2024; Accepted: May 09, 2024

REFERENCES

1. Bhatt S, Gething PW, Brady OJ, Messina JP, Farlow AW, Moyes CL, et al. The global distribution and burden of dengue. Nature 2013;496(7446):504 – 7. https://doi.org/10.1038/nature12060.
2. Brady OJ, Gething PW, Bhatt S, Messina JP, Brownstein JS, Hoen AG, et al. Refining the global spatial limits of dengue virus transmission by evidence-based consensus. PLoS Negl Trop Dis 2012;6(8):e1760. https://doi.org/10.1371/journal.pntd.0001760.
3. Wu JY, Lun ZR, James AA, Chen XG. Dengue Fever in mainland China. Am J Trop Med Hyg 2010;83(3):664 – 71. https://doi.org/10.4269/ajtmh.2010.09-0755.
4. Yue YJ, Liu XB, Xu M, Ren DS, Liu QY. Epidemiological dynamics of dengue fever in mainland China, 2014-2018. Int J Infect Dis 2019;86:82 – 93. https://doi.org/10.1016/j.ijid.2019.06.015.
5. Yue YJ, Liu QY, Liu XB, Zhao N, Yin WW. Dengue fever in mainland China, 2005-2020: a descriptive analysis of dengue cases and *Aedes* data. Int J Environ Res Public Health 2022;19(7):3910. https://doi.org/10.3390/ijerph19073910.
6. Li HX, Zhou HN, Yang YC, Jiang H. Dengue fever epidemic situation in Yunnan province from 2004 to 2008. Chin J Vector Biol Control 2010;21(6):576-7,580. https://d.wanfangdata.com.cn/periodical/zgmjswxjkzzz201006017. (In Chinese).
7. Wang BH, Yang HL, Feng Y, Zhou HN, Dai JJ, Hu YZ, et al. The distinct distribution and phylogenetic characteristics of dengue virus serotypes/genotypes during the 2013 outbreak in Yunnan, China: Phylogenetic characteristics of 2013 dengue outbreak in Yunnan, China. Infect Genet Evol 2016;37:1 – 7. https://doi.org/10.1016/j.meegid.2015.10.022.
8. Wang BH, Li YP, Feng Y, Zhou HN, Liang YB, Dai JJ, et al. Phylogenetic analysis of dengue virus reveals the high relatedness between imported and local strains during the 2013 dengue outbreak in Yunnan, China: a retrospective analysis. BMC Infect Dis 2015;15:142. https://doi.org/10.1186/s12879-015-0908-x.
9. Hu TS, Zhang HL, Feng Y, Fan JH, Tang T, Liu YH, et al. Epidemiological and molecular characteristics of emergent dengue virus in Yunnan Province near the China-Myanmar-Laos border, 2013-2015. BMC Infect Dis 2017;17(1):331. https://doi.org/10.1186/s12879-017-2401-1.
10. Zhang J, Shu Y, Shan XY, Li DY, Ma DH, Li TT, et al. Co-circulation of three dengue virus serotypes led to a severe dengue outbreak in Xishuangbanna, a border area of China, Myanmar, and Laos, in 2019. Int J Infect Dis 2021;107:15 – 7. https://doi.org/10.1016/j.ijid.2021.04.010.
11. Liu YH, Yin XX, Zhang HL, Yang ZL, Dong CL, Chen SY, et al. Epidemiological characteristics of dengue fever and monitoring of Aedes vector mosquitoes in Dehong Dai and Jingpo Autonomous Prefecture of Yunnan province, China, 2013-2019. Chin J Vector Biol Control 2021;32(2):173 – 80. https://doi.org/10.11853/j.issn.1003.8280.2021.02.011.
12. Zhang HL, Zhang YZ, Yang WH, Feng Y, Nasci RS, Yang J, et al. Mosquitoes of Western Yunnan Province, China: seasonal abundance, diversity, and arbovirus associations. PLoS One 2013;8(10):e77017. https://doi.org/10.1371/journal.pone.0077017.
13. Liang GD, Li XL, Gao XY, Fu SH, Wang HY, Li MH, et al. Arboviruses and their related infections in China: a comprehensive field and laboratory investigation over the last 3 decades. Rev Med Virol 2018;28(1):e1959. https://doi.org/10.1002/rmv.1959.
14. Lv RC, Zhu CQ, Wang CH, Ai LL, Lv H, Zhang B, et al. Genetic diversity and population structure of *Aedes aegypti* after massive vector control for dengue fever prevention in Yunnan border areas. Sci Rep 2020;10(1):12731. https://doi.org/10.1038/s41598-020-69668-7.
15. Li NZ, Feng Y, Vrancken B, Chen YY, Dong L, Yang QQ, et al. Assessing the impact of COVID-19 border restrictions on dengue transmission in Yunnan Province, China: an observational epidemiological and phylogenetic analysis. Lancet Reg Health West Pac 2021;14:100259. https://doi.org/10.1016/j.lanwpc.2021.100259.

SUPPLEMENTARY MATERIAL

SUPPLEMENTARY TABLE S1. Distribution of dengue fever cases across prefectures and cities in Yunnan Province, China, 2010–2021.

City	2010	2011	2012	2013	2014	2015	2016	2017	2018	2019	2020	2021	Total	Component ratio (%)
Xishuangbanna	6	4	14	1,327	1	1,141	32	1,356	637	4,126	1	0	8,645	61.32
Dehong	0	1	1	193	188	448	279	837	98	1,271	240	11	3,567	25.30
Lincang	0	0	0	0	1	196	1	319	43	587	2	0	1,149	8.15
Kunming	8	7	5	14	15	13	11	22	34	166	4	2	301	2.14
Honghe	0	0	0	0	0	3	0	5	2	125	1	0	136	0.96
Baoshan	0	0	0	2	3	3	1	23	4	38	0	0	74	0.52
Zhaotong	0	0	0	0	2	1	0	4	10	43	1	0	61	0.43
Puer	3	0	2	0	0	3	1	2	2	45	0	0	58	0.41
Qujing	1	1	1	0	1	2	0	3	3	29	0	0	41	0.29
Dali	0	0	0	1	1	2	0	1	4	19	0	0	28	0.20
Chuxiong	0	0	0	0	1	0	0	2	2	8	0	0	13	0.09
Yuxi	0	0	0	0	0	3	0	0	2	6	0	0	11	0.08
Wenshan	0	0	0	0	0	0	0	0	1	5	1	0	7	0.05
Lijiang	0	0	0	1	0	1	0	0	0	3	0	0	5	0.04
Nujiang	0	0	0	0	0	0	0	1	0	0	0	0	1	0.01
Diqing	0	0	0	0	0	0	0	0	0	0	0	0	0	0.00
Unknown	0	0	1	0	0	0	0	0	0	0	0	0	1	0.01
Total	18	13	24	1,538	213	1,816	325	2,575	842	6471	250	13	14,098	100.00

SUPPLEMENTARY TABLE S2. Dengue fever cases by district and county in Yunnan Province, 2010–2021.

County	Cumulative cases	Indigenous cases	Overseas imported cases	Imported cases from other PLADs
Wuhua District	48	0	48	0
Panlong District	43	0	43	0
Guandu District	115	0	112	3
Xishan District	49	0	48	1
Dongchuan District	4	0	4	0
Chenggong District	9	0	9	0
Jinning District	2	0	2	0
Fumin County	3	0	3	0
Yiliang County	6	0	6	0
Shilin Yi Autonomous County	1	0	1	0
Songming County	7	0	7	0
Luchuan Yi and Miao Autonomous County	4	0	4	0
Xundian Hui and Yi Autonomous County	2	0	2	0
Anning City	4	0	4	0
Qilin District	6	0	6	0
Zhanyi District	2	0	2	0
Malong District	0	0	0	0
Luliang County	3	0	3	0
Shizong County	3	0	3	0

Continued

County	Cumulative cases	Indigenous cases	Overseas imported cases	Imported cases from other PLADs
Luoping County	5	0	5	0
Fuyuan County	4	0	3	1
Huize County	6	0	6	0
Xuanwei City	12	0	12	0
Hongta District	2	0	2	0
Jiangchuan District	3	0	3	0
Tonghai County	2	0	2	0
Huaning County	0	0	0	0
Yimen County	1	0	1	0
Eshan Yi Autonomous County	1	0	1	0
Xinping Yi and Dai Autonomous County	0	0	0	0
Yuanjiang Hani, Yi, and Dai Autonomous County	0	0	0	0
Chengjiang City	2	0	2	0
Longyang District	12	0	12	0
Shidian County	6	0	6	0
Longling County	11	0	11	0
Changning County	0	0	0	0
Tengchong City	45	0	44	1
Zhaoyang District	4	0	4	0
Ludian County	3	0	3	0
Qiaojia County	2	0	2	0
Yanjin County	4	0	4	0
Daguan County	0	0	0	0
Yongshan County	2	0	2	0
Suijiang County	1	0	1	0
Zhenxiong County	41	0	40	1
Yiliang County	1	0	1	0
Weixin County	2	0	2	0
Shuifu City	1	0	1	0
Gucheng District	0	0	0	0
Yulong Naxi Autonomous County	2	0	2	0
Yongsheng County	3	0	2	1
Huaping County	0	0	0	0
Ninglang Yi Autonomous County	0	0	0	0
Simao District	8	0	8	0
Ninger Hani and Yi Autonomous County	0	0	0	0
Mojiang Hani Autonomous County	0	0	0	0
Jingdong Yi Autonomous County	3	0	3	0
Jinggu Dai and Yi Autonomous County	2	0	2	0
Zhenyuan Yi, Hani and Lahu Autonomous County	0	0	0	0
Jiangcheng Hani and Yi Autonomous County	5	3	2	0
Menglian Dai, Lahu and Wa Autonomous County	37	15	22	0

Continued

County	Cumulative cases	Indigenous cases	Overseas imported cases	Imported cases from other PLADs
Lancang Lahu Autonomous County	2	0	2	0
Ximeng Wa Autonomous County	1	0	1	0
Linxiang District	4	0	4	0
Fengqing County	7	0	7	0
Yun County	3	0	3	0
Yongde County	12	0	12	0
Zhenkang County	312	0	312	0
Shuangjiang Lahu, Wa, Bulang, and Dai Autonomous County	2	0	2	0
Gengma Dai and Wa Autonomous County	802	502	299	1
Cangyuan Wa Autonomous County	7	0	7	0
Chuxiong City	3	0	3	0
Shuangbai County	0	0	0	0
Mouding County	4	0	4	0
Nanhua County	1	0	0	1
Yao'an County	2	0	2	0
Dayao County	1	0	1	0
Yongren County	0	0	0	0
Yuanmou County	0	0	0	0
Wuding County	1	0	1	0
Lufeng County	1	0	1	0
Gejiu City	1	0	1	0
Kaiyuan City	3	0	3	0
Mengzi City	3	0	3	0
Mile City	5	0	5	0
Pingbian Miao Autonomous County	1	0	1	0
Jianshui County	0	0	0	0
Shiping County	0	0	0	0
Luxi County	1	0	1	0
Yuanyang County	1	0	1	0
Honghe County	0	0	0	0
Jinping Miao, Yao and Dai Autonomous County	3	0	3	0
Luchun County	1	0	1	0
Hekou Yao Autonomous County	117	114	3	0
Wenshan City	1	0	1	0
Yanshan County	3	0	3	0
Xichou County	0	0	0	0
Malipo County	0	0	0	0
Maguan County	0	0	0	0
Qiubei County	0	0	0	0
Guangnan County	2	0	1	1
Funing County	1	0	0	1
Jinghong City	7,668	7,571	95	2

Continued

County	Cumulative cases	Indigenous cases	Overseas imported cases	Imported cases from other PLADs
Menghai County	211	0	211	0
Mengla County	765	650	115	0
Dali City	5	0	5	0
Yangbi Yi Autonomous County	0	0	0	0
Xiangyun County	6	0	6	0
Binchuan County	3	0	2	1
Midu County	2	0	2	0
Nanjian Yi Autonomous County	2	0	2	0
Weishan Yi and Hui Autonomous County	1	0	1	0
Yongping County	0	0	0	0
Yunlong County	2	0	2	0
Eryuan County	6	0	6	0
Jianchuan County	1	0	1	0
Heqing County	0	0	0	0
Ruili City	3,262	2,620	641	3
Mang City	51	18	33	0
Lianghe County	10	0	7	1
Yingjiang County	161	7	154	0
Longchuan County	83	13	70	0
Lushui City	0	0	0	0
Fugong County	0	0	0	0
Gongshan Derung and Nu Autonomous County	0	0	0	0
Lanping Bai and Pumi Autonomous County	1	0	1	0
Shanggelila City	0	0	0	0
Deeqeen County	0	0	0	0
Weixi Lisu Autonomous County	0	0	0	0
Unknown	6	0	6	0
Total	14,098	11,513	2,566	19

SUPPLEMENTARY TABLE S3. Countries of origin and number of dengue cases imported into Yunnan Province, 2010–2021.

City	2010	2011	2012	2013	2014	2015	2016	2017	2018	2019	2020	2021	Total	Component ratio (%)
Myanmar	1	2	2	65	59	285	91	618	101	707	5	1	1,937	75.49
Cambodia	0	0	0	0	0	0	1	0	42	222	2	0	267	10.41
Laos	7	4	13	14	0	5	5	32	2	115	1	1	199	7.76
Thailand	0	0	3	8	2	10	5	4	12	18	0	0	62	2.42
Africa	0	2	1	3	7	1	2	1	0	8	2	0	27	1.05
Vietnam	0	0	0	0	0	2	0	5	2	12	2	0	23	0.90
Malaysia	0	0	0	0	1	2	2	1	0	3	0	0	9	0.35
Sri Lanka	0	0	0	0	0	2	1	2	2	0	0	1	8	0.31
India	1	0	2	0	0	0	0	1	0	2	0	0	6	0.23
Bangladesh	0	0	0	0	0	1	0	1	0	1	0	0	3	0.12
Maldives	0	0	0	0	0	0	0	0	2	1	0	0	3	0.12
Philippines	0	0	0	0	0	0	0	0	0	2	1	0	3	0.12
Indonesia	0	0	0	0	0	0	1	0	0	0	0	0	1	0.04
Unknown	9	5	3	1	0	0	0	0	0	0	0	0	18	0.70
Total	18	13	24	91	69	308	108	665	163	1,091	13	3	2,566	100.00

SUPPLEMENTARY TABLE S4. Spatial global autocorrelation analysis of dengue fever in Yunnan Province, China, 2010–2021.

Year	Moran's I	Z	*P*
2010	0.427	9.019	<0.001
2011	0.019	0.556	0.527
2012	0.581	13.761	<0.001
2013	0.05	2.010	0.044
2014	−0.002	2.249	0.025
2015	0.008	0.389	0.697
2016	0.016	4.079	<0.001
2017	0.172	4.535	<0.001
2018	0.107	3.510	<0.001
2019	0.128	3.240	0.001
2020	0.000074	3.324	<0.001
2021	−0.003	1.403	0.161

SUPPLEMENTARY TABLE S5. Hot spots of dengue fever annual incidence in Yunnan Province, China.

Year	Hotspot	
	Number	County
2010	5	Jinghong, Mengla, Simao, Chenggong, Panlong
2011	5	Jinghong, Ruili, Wuhua, Anning, Jinning
2012	4	Jinghong, Mengla, Jiangcheng, Ruili
2013	2	Jinghong, Ruili
2014	1	Ruili
2015	3	Jinghong, Ruili, Gengma
2016	1	Ruili
2017	4	Jinghong, Ruili, Mengla, Gengma
2018	4	Jinghong, Mengla, Menghai, Simao
2019	3	Jinghong, Mengla, Ruili
2020	1	Ruili
2021	1	Ruili

SUPPLEMENTARY TABLE S6. Analysis of temporal and spatial scanning results of dengue fever incidence in Yunnan Province, China, 2010–2021.

Type	Number	Radius (km)	Time frame	Cases	Expected cases	Population	*RR*	*LLR*	*P*
Most likely cluster	2	69.29	2015–2019	7,085	94.07	732,398	150.46	25770.59	<0.001
Secondary likely cluster 1	54	277.33	2010–2015	71	3521.99	22,853,680	0.015	3684.24	<0.001
Secondary likely cluster 2	29	181.40	2017–2019	3,236	732.51	9,510,581	5.44	2554.75	<0.001

Abbreviation: RR=relative risk; LLR=log-likelihood ratio.

Methods and Applications

Exploration for the Priority of HIV Intervention: Modelling Health Impact and Cost-Effectiveness — Six Cities, Eastern China, 2019–2028

Youran Zhang[1]; Lili Wang[1]; Zhen Jiang[2,#]; Hongjing Yan[3]; Xiaoxia Liu[4]; Jing Gu[5]; Guoyong Wang[6];
Xiaosong Cheng[7]; Qiyan Leng[7]; Qisui Long[8]; Zimian Liang[9]; Jing Wang[9]; Liang Liang[10];
Yanchao Qiu[11]; Lin Chen[12]; Hang Hong[13]

ABSTRACT

Introduction: In order to enhance the effectiveness of resource allocation, regions must tailor their responses to their specific epidemiological and economic situations.

Methods: Utilizing Spectrum software, we projected the cost-effectiveness of 10 chosen HIV interventions in six cities in eastern China from 2019 to 2028. We assessed three scenarios — Base, Achievable, and Idealized — for each city. The analysis included the projected number of HIV infections and deaths averted, as well as the incremental cost-effectiveness ratios for each intervention in the six cities.

Results: In Shijiazhuang, Wuxi, Yantai, and Zhenjiang, cities with initially low antiretroviral therapy (ART) coverage, ART showed significant effectiveness, especially for males. Conversely, in Foshan and Ningbo, where ART coverage was notably high, oral pre-exposure prophylaxis (PrEP) for men who have sex with men (MSM) proved effective in the Idealized scenario. MSM outreach, ART for males, and ART for females demonstrated cost-effectiveness across all six cities in both Achievable and Idealized scenarios at the predefined thresholds for each city.

Discussion: Maintaining an appropriate coverage rate for outreach to MSM can lead to cost-effectiveness. In cities with low ART coverage, scaling up ART remains a crucial intervention. In regions with high ART coverage, consideration may be given to the utilization of oral PrEP for MSM individuals, requiring budget allocation.

To effectively implement customized interventions, each region and country must address their unique epidemiological and economic situations and establish key actions to enhance local human immunodeficiency virus (HIV) responses. Creating tailored financial strategies for sustainability is crucial to guarantee universal access and better health results. Progress evaluation should encompass a comprehensive spectrum of HIV interventions to benefit all demographic groups.

Studies using Spectrum modules have shown that HIV intervention programs are cost-effective in regions like sub-Saharan Africa, Asia, and the Caribbean (*1*–*4*). Nonetheless, due to the significant variability in HIV prevalence and intervention coverage in eastern China, it is challenging to extrapolate these results to that specific area.

This study aims to forecast the health outcomes and cost-effectiveness of scaling up HIV interventions, and to prioritize life-saving HIV interventions in six cities in eastern China, utilizing the Spectrum modules.

METHODS

Five cities in eastern China, namely Foshan, Ningbo, Shijiazhuang, Wuxi, and Yantai, were chosen based on the following criteria: each city had a total population exceeding three million and reported over 200 new cases of HIV infection annually. To simultaneously assess the cost-effectiveness discrepancies between two cities within the same province and provide insights for subsequent spatiotemporal distribution studies, Zhenjiang — an additional city in Jiangsu Province like Wuxi, boasting a population of three million and approximately 50 newly reported HIV cases each year — was included in the analysis (*5*).

A standardized data collection tool was developed following the Spectrum framework to calculate costs and model healthcare payer perspectives. Data from public and service sectors in six cities between 2015 and 2019 were collected. This study investigates the cost-effectiveness of 10 key HIV interventions (Table 1) and presents the HIV intervention priorities across sampled cities for the period 2019–2028.

Three scenarios were simulated to project the outcomes of scaling up interventions in each city, under the assumption of an unlimited budget.

Scenario 1: Base Scenario

In the Base scenario, from 2020 to 2028, all interventions maintain the same coverage as in 2019.

Scenario 2: Achievable Scenario

Enhance the scope of specific interventions by double up to 99.90% by 2028, with the exception of oral pre-exposure prophylaxis (PrEP) for high-risk heterosexual (HRH) individuals and men who have sex with men (MSM) due to the absence of prior testing and coverage in the studied cities. Simultaneously, escalate the coverage of oral PrEP for HRH and MSM from 0% in the starting year to 5% by 2028. Linear interpolation was utilized to project the coverage rates between 2020 and 2027, while the coverage for other interventions remained constant from 2019.

Scenario 3: Idealized Scenario

In this case, it was assumed that the coverage rate of the 10 chosen interventions would reach 99.90%. Linear interpolation was used to simulate the coverage rates for the years 2020–2027. The coverage rates of the remaining interventions were held constant at 2019 levels.

Definitions of the 10 selected intervention coverage and the remaining interventions's coverage all displayed in the Supplementary Table S1 (available at https://weekly.chinacdc.cn/). The Coverage assumptions for 10 selected HIV interventions in the target year 2028 were displayed in Supplementary Table S2 (available at https://weekly.chinacdc.cn/). Unit costs for each intervention were based on local data from six cities in 2019 and kept constant in the model, as outlined in Supplementary Table S3 (available at https://weekly.chinacdc.cn/).

Initially, the model simultaneously expanded the coverage of ten selected interventions to determine the total infections and deaths prevented, as well as the costs for each scenario in each city. Subsequently, each intervention was individually scaled up per scenario in every city to analyze the outcomes of each intervention.

Output Indicators

The number of infections and deaths prevented by scaling up interventions from the Base scenario to the Achievable or Idealized scenarios was directly derived from the model calculations. Costs for each scenario, presented in 2019 Chinese Yuan (CNY) with a 3% annual discount rate and an exchange rate of 1 USD=6.90 CNY (*6*), were calculated. Incremental cost was manually determined by comparing intervention costs under the Achievable or Idealized scenarios with those under the Base scenario. The incremental cost-effectiveness ratio (ICER) was calculated as the ratio of incremental costs to infections averted. To account for economic variations across cities, cost-effective interventions in each city were classified as those with an ICER below the 2019 per capita GDP

TABLE 1. Coverage of 10 selected interventions in six cities in 2019.

Selected interventions (% per year)	Foshan	Ningbo	Shijiazhuang	Wuxi	Yantai	Zhenjiang
VCT	0.22	0.31	0.40	0.14	0.41	0.49
Condoms for adult population	0	25.41	18.75	39.09	20.48	0
SSTT	99.90	95.00	2.50	3.00	0.00	1.40
FSW outreach	99.90	72.00	28.34	99.90	92.00	94.00
MSM outreach	79.32	59.20	70.00	29.94	92.70	4.80
MSM receiving lubricants	79.32	0	11.21	9.98	7.20	3.90
Oral PrEP for HRH	0	0	0	0	0	0
Oral PrEP for MSM	0	0	0	0	0	0
ART for males	99.90	99.90	50.86	86.14	38.61	79.48
ART for females	99.90	99.90	16.93	42.58	10.75	49.90

Abbreviation: VCT=voluntary counseling and testing for adult population; SSTT=secondary students with teachers trained in AIDS; FSW=female sex worker; MSM=men who have sex with men; PrEP=pre-exposure prophylaxis; HRH=high risk heterosexual; ART=antiretroviral therapy.

(Supplementary Table S4, available at https://weekly.chinacdc.cn/) for that city per infection averted.

Sensitivity Analysis

A one-way sensitivity analysis was performed by adjusting the unit cost of selected interventions by +/-50% of the original values to assess the model's stability.

RESULT

Table 2 illustrates the comprehensive costs and cost-effectiveness of two distinct scenarios across six cities from 2019 to 2028. During this period, under the Achievable scenario with Shijiazhuang reaching optimal impact, a total of 1,580 HIV infections and 550 deaths were prevented. In contrast, the Idealized scenario showed even greater impact, with 2,608 HIV infections and 796 deaths averted. The least impact was noted in Foshan and Ningbo. As anticipated, the costs per infection and death averted in the Idealized scenario were considerably higher compared to those in the Achievable scenario across all six cities. In municipalities with high initial antiretroviral therapy (ART) coverage, like Foshan and Ningbo, the ICERs were significant, yielding 0.47 million yuan per infection averted in the Achievable scenario and exceeding 100 million yuan in the Idealized scenario, indicating poor cost-effectiveness when scaling up interventions. Conversely, in the other four cities with lower initial ART coverage, such as Shijiazhuang and Yantai, escalating current intervention coverage proved to be highly cost-effective, adhering to the cost-effectiveness thresholds established for these cities within the Achievable scenario.

Figure 1 and Table 3 display the cost-effectiveness of HIV interventions in six cities under Achievable and Idealized scenarios. In cities like Shijiazhuang, Wuxi, Yantai, and Zhenjiang, ART, especially for males, showed high effectiveness in averting infections. The most impactful strategy was ART for males in Shijiazhuang, projected to prevent 1,367 infections from 2019 to 2028. The majority of prevented deaths were attributed to ART based on the Spectrum framework (Supplementary Table S5, available at https://weekly.chinacdc.cn/). In Foshan and Ningbo, with high ART coverage, oral PrEP for MSM in the Idealized scenario demonstrated significant effectiveness.

At the cost-effectiveness threshold of each city, interventions such as outreach to MSM, ART for males, and ART for females were found to be cost-effective across six cities in both scenarios. Among these, MSM outreach was identified as the most cost-effective, with a range between 0.39 to 42.48 thousand yuan per infection averted. However, the effectiveness of MSM outreach may plateau with expanded coverage, as depicted in Figure 1. For instance, in Zhenjiang and Wuxi, the number of HIV infections averted through MSM outreach increased significantly from Achievable to Idealized scenarios, while the impact in the other four cities did not show a further increase with scaled-up coverage.

TABLE 2. Overall costs and cost-effectiveness in the Achievable Scenario and the Idealized Scenario among six cities from 2019 to 2028.

Cost and health impact		Foshan	Ningbo	Shijiazhuang	Wuxi	Yantai	Zhenjiang
Total cost of Base Scenario (Million CNY)		141.05	203.55	443.48	202.16	156.53	82.36
Total cost of Achievable Scenario (Million CNY)		145.16	212.53	473.88	222.13	171.50	86.70
Total cost of Idealized Scenario (Million CNY)		375.62	1,054.31	866.18	684.72	915.93	444.30
Total number of infections averted	AS	9	19	1,580	335	618	284
	IS	118	131	2,608	477	1,618	401
Total number of deaths averted	AS	0*	0*	550	132	469	61
	IS	1	1	796	156	775	61
Incremental cost per infection averted (Million CNY)	AS	0.47	0.47	0.02	0.06	0.02	0.02
	IS	1.98	6.51	0.16	1.01	0.47	0.90
Incremental cost per death averted (Million CNY)	AS	105.62	103.20	0.06	0.15	0.03	0.07
	IS	436.82	1,432.25	0.53	3.10	0.98	5.89

Abbreviation: AS=Achievable Scenario; IS=Idealized Scenario; CNY=Chinese Yuan.

* indicates that the numbers provided are rounded integers. The total deaths averted in Foshan and Ningbo were 0.039 and 0.087, respectively.

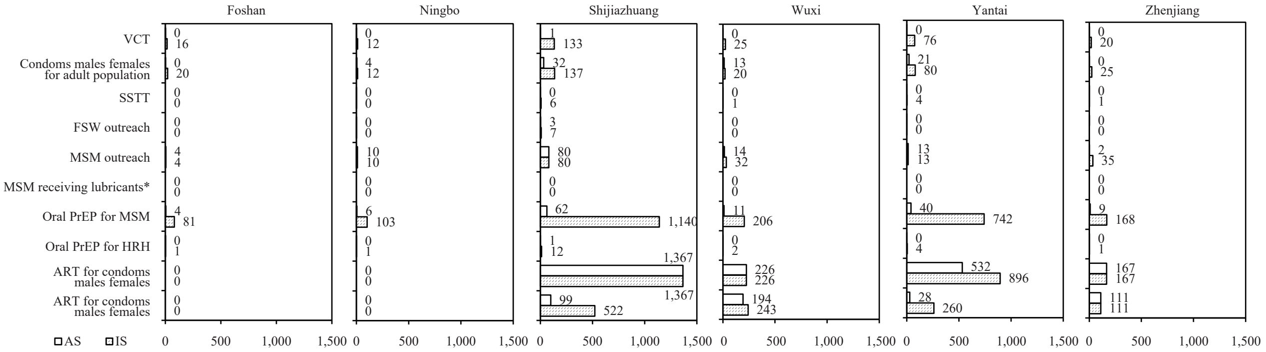

FIGURE 1. Total HIV infections averted by 10 selected HIV interventions in Achievable and Idealized Scenarios in six cities from 2019 to 2028.

Abbreviation: VCT=Voluntary counseling and testing for adult population; SSTT=Secondary students with teachers trained in AIDS; FSW=Female sex worker; MSM=Men who have sex with men; PrEP=Pre-exposure prophylaxis; HRH=High risk heterosexual; ART=Antiretroviral therapy; AS= Achievable Scenario; IS=Idealized Scenario.

* indicates that the impact of MSM receiving lubricants was modeled as 0 in six cities.

TABLE 3. Incremental cost per HIV infection averted for 10 selected HIV interventions in two scenarios across six cities from 2019 to 2028 (thousand CNY).

Selected interventions	Foshan		Ningbo		Shijiazhuang		Wuxi		Yantai		Zhenjiang	
	AS	IS	AS	IS	AS	IS	AS	IS	AS	IS	AS	IS
VCT	53,976.14	9,265.54	60,648.14	62,654.05	1,697.46	1,756.36	15,228.19	15,783.12	8,355.87	8,588.52	105,931.86	16,552.63
Condoms for adult population	1,242.07	1,537.69	237.21	241.46	265.94	272.39	564.35	571.22	47.04*	48.05*	9.05*	28.91*
SSTT	−	−	3,941.67	3,941.67	253.34	263.72	1,376.34	1,491.83	488.55	501.79	1,814.65	1,661.12
FSW outreach	−	−	2,271.00	2,271.00	36.64*	37.49*	−	−	40.63*	40.63*	11.85*	11.85*
MSM outreach	33.06*	33.06*	42.48*	42.48*	0.39*	0.39*	19.76*	19.99*	1.70*	1.70*	6.27*	6.49*
MSM receiving lubricants	−	−	−	−	−	−	−	−	−	−	−	−
Oral PrEP for HRH	68,969.20	67,956.75	115,145.91	114,166.19	9,481.25	9,505.91	35,247.30	35,593.72	18,679.28	18,630.42	27,134.91	27,549.97
Oral PrEP for MSM	147.08*	159.14*	181.99	194.71	15.40*	17.94*	57.63*	64.17*	16.22*	18.59*	33.65*	37.78*
ART for males	−	−	−	−	9.75*	9.75*	19.09*	19.09*	12.30*	12.13*	4.26*	4.26*
ART for females	−	−	−	−	8.66*	12.53*	15.27*	17.89*	18.51*	22.34*	2.61*	2.62*

Note: “−” indicates that the impact was 0 and cannot be divided.

Abbreviation: VCT=Voluntary counseling and testing for adult population; SSTT=Secondary students with teachers trained in AIDS; FSW=Female sex worker; MSM=Men who have sex with men; PrEP=Pre-exposure prophylaxis; HRH=High risk heterosexual; ART=Antiretroviral therapy; AS= Achievable Scenario; IS=Idealized Scenario.

* indicates that the intervention in this city was cost-effective at the threshold level of this city.

The results indicate that the epidemiological efficacy of the intervention is influenced by the coverage levels in different scenarios. Supplementary Table S6 (available at https://weekly.chinacdc.cn/) presents the cost per HIV infection averted based on varying unit costs of interventions. A direct correlation was observed between unit cost and cost per HIV infection averted; a 50% decrease in unit cost resulted in a similar decrease in the cost per HIV infection averted, and vice versa (Supplementary Table S7, available at https://weekly.chinacdc.cn/).

DISCUSSION

Our research conducted using the Spectrum model offers valuable insights for guiding resource allocation. Between 2019 and 2028, Shijiazhuang demonstrated the highest potential impact with the lowest ICER compared to other cities analyzed. Situated in Hebei province, Shijiazhuang stands out due to its large population of 11 million, low ART coverage, and limited HIV resources per capita. In contrast, Foshan had the lowest estimated potential impact, while Ningbo had the highest ICER. These cities, located in prosperous provinces like Guangdong and Zhejiang, exhibit high ART coverage and ample HIV resources. Therefore, prioritizing funding towards regions with growing economies, low treatment rates, and substantial populations is crucial in shaping the future of HIV intervention strategies (*7*).

The study showcased that transitioning from an Achievable to an Idealized scenario for a single intervention coverage results in a minor health impact change at a significantly higher cost. For instance, the ICER in the Idealized scenario is estimated to be approximately 4 times (in Foshan) to 45 times (in Zhenjiang) greater compared to the Achievable scenario. Thus, opting for an Achievable scenario is advisable for policymakers with constrained resources across the six cities.

The results guide the development of a ten-year priority intervention plan for six cities, including MSM outreach, ART for males, and ART for females. Prior research has shown that MSM outreach significantly enhances HIV testing rates (*8*) and encourages prompt treatment (*9*). However, there is limited data on the cost-effectiveness of MSM outreach (*10*). Our study indicated that the impact of MSM outreach on health outcomes plateaued at a baseline coverage of around 59.2% (in Ningbo). Beyond this threshold, supplementary interventions are necessary to address remaining gaps due to the saturation of MSM outreach.

ART has proven to be the most effective and economical approach for reducing HIV infections and mortalities in Shijiazhuang, Wuxi, Yantai, and Zhenjiang. In contrast, oral PrEP for MSM has emerged as the strategy of choice in Foshan and Ningbo, areas with high ART coverage, to meet the objectives of decreasing new HIV infections. These findings align with previous oral PrEP modeling studies (*11–12*). Nonetheless, the adoption of this strategy in Ningbo, where the ICER soared to 181.99 and 194.71 thousand yuan per infection averted, was deemed not cost-effective according to the city's threshold of 146.12 thousand yuan per infection averted. While extensive ART coverage may significantly curb HIV transmission, rendering PrEP redundant and uneconomical in such cases (*13*), the indirect benefits of enhanced HIV testing and linkage to subsequent treatment attributable to PrEP cannot be overlooked (*14*). Given the substantial public health challenge posed by the prevalence of HIV among MSM in China, it is imperative that economically developed areas with high ART coverage continuously evaluate and expand oral PrEP for MSM, ensuring sufficient budgetary provisions. To achieve the ambitious aim of halting the HIV epidemic, strategies must be meticulously tailored and implemented at the local level.

Like all modeling studies, this study is subject to some limitations. First, due to insufficient regional data, we utilized some national-level indicators in the model, potentially impacting the accuracy of projections. Second, the lack of data on mobile populations could lead to underestimation of local epidemics. Third, our models did not consider the impacts of disruptions related to coronavirus disease 2019 (COVID-19) (*15*). While COVID-19 does not directly influence HIV transmission biologically, it does affect various factors such as awareness, behavior, and healthcare resource availability, as well as resource allocation in response to the sporadic nature of the epidemic.

In conclusion, this study by Spectrum delineated key actions for regions sampled from 2019 to 2028 to improve HIV response and achieve optimal health outcomes in AIDS control. The utilization of Spectrum is crucial for guiding prioritization in cities based on their unique epidemiological, economic, and HIV response characteristics.

Conflicts of interest: No conflicts of interest.

Acknowledgements: Thank the staff from Jiangsu Provincial CDC, Guangdong Provincial CDC, Zhejiang Provincial CDC, Shandong Provincial CDC, Hebei Provincial CDC, Shijiazhuang CDC, Yantai CDC, Ningbo CDC, Zhenjiang CDC, Foshan CDC, and Wuxi CDC for their assistance in data collection and verification.

Funding: Supported by the National Science Foundation of China (Grant No. 71874169).

doi: 10.46234/ccdcw2024.089

$^{\#}$ Corresponding author: Zhen Jiang, jiangzhen@chinaaids.cn.

---

[1] School of Health Service Management, Anhui Medical University, Hefei City, Anhui Province, China; [2] Division of Prevention and intervention, National Center for AIDS and STD Control and Prevention, Chinese Center for Disease Control and Prevention, Beijing, China; [3] Jiangsu Provincial Center for Disease Control and Prevention, Nanjing City, Jiangsu Province, China; [4] Zhenjiang Center for Disease Control and Prevention, Zhenjiang City, Jiangsu Province, China; [5] Wuxi Center for Disease Control and Prevention, Wuxi City, Jiangsu Province, China; [6] Shandong Provincial Center for Disease Control and Prevention, Jinan City, Shandong Province, China; [7] Yantai Center for Disease Control and Prevention, Yantai City, Shandong Province, China; [8] Guangdong Provincial Center for Disease Control and Prevention, Guangzhou City, Guangdong Province,

China; [9] Foshan Center for Disease Control and Prevention, Foshan City, Guangdong Province, China; [10] Hebei Provincial Center for Disease Control and Prevention, Shijiazhuang City, Hebei Province, China; [11] Shijiazhuang Center for Disease Control and Prevention, Shijiazhuang City, China; [12] Zhejiang Provincial Center for Disease Control and Prevention, Hangzhou City, Zhejiang Province, China; [13] Ningbo Center for Disease Control and Prevention, Ningbo City, Zhejiang Province, China.

Submitted: February 26, 2024; Accepted: May 08, 2024

REFERENCES

1. Kripke K, Eakle R, Cheng A, Rana S, Torjesen K, Stover J. The case for prevention - Primary HIV prevention in the era of universal test and treat: a mathematical modeling study. EClinicalMedicine 2022;46: 101347. https://doi.org/10.1016/j.eclinm.2022.101347.
2. Kapiriri L, Lee NM, Wallace LJ, Kwesiga B. Beyond cost-effectiveness, morbidity and mortality: a comprehensive evaluation of priority setting for HIV programming in Uganda. BMC Public Health 2019;19(1): 359. https://doi.org/10.1186/s12889-019-6690-8.
3. Atun R, Chang AY, Ogbuoji O, Silva S, Resch S, Hontelez J, et al. Long-term financing needs for HIV control in sub-Saharan Africa in 2015-2050: a modelling study. BMJ Open 2016;6(3):e009656. https://doi.org/10.1136/bmjopen-2015-009656.
4. Kasaie P, Weir B, Schnure M, Dun C, Pennington J, Teng Y, et al. Integrated screening and treatment services for HIV, hypertension and diabetes in Kenya: assessing the epidemiological impact and cost-effectiveness from a national and regional perspective. J Int AIDS Soc 2020;23 Suppl 1(Suppl 1):e25499. http://dx.doi.org/10.1002/jia2.25499.
5. Zhang YR, Wang LL, Jiang Z, Yan HJ, Liu XX, Gu J, et al. Estimating costs of the HIV comprehensive intervention using the spectrum model - China, 2015-2019. China CDC Wkly 2022;4(25):554 – 9. https://doi.org/10.46234/ccdcw2022.119.
6. The People's Bank of China. Chart of CNY exchange rate midpoint. http://www.pbc.gov.cn/rmyh/108976/109428/index.html. [2022-6-26]. (in Chinese).
7. Sahu D, Kumar P, Chandra N, Rajan S, Shukla DK, Venkatesh S, et al. Findings from the 2017 HIV estimation round & trend analysis of key indicators 2010-2017: evidence for prioritising HIV/AIDS programme in India. Indian J Med Res 2020;151(6):562 – 70. https://doi.org/10.4103/ijmr.IJMR_1619_19.
8. Sundararajan R, Ponticiello M, Nansera D, Jeremiah K, Muyindike W. Interventions to increase HIV testing uptake in global settings. Curr HIV/AIDS Rep 2022;19(3):184 – 93. https://doi.org/10.1007/s11904-022-00602-4.
9. Colvin CJ. Strategies for engaging men in HIV services. Lancet HIV 2019;6(3):e191 – 200. https://doi.org/10.1016/S2352-3018(19)30032-3.
10. Yeh PT, Kennedy CE, Minamitani A, Baggaley R, Shah P, Verster A, et al. Web-based service provision of HIV, viral hepatitis, and sexually transmitted infection prevention, testing, linkage, and treatment for key populations: systematic review and meta-analysis. J Med Internet Res 2022;24(12):e40150. https://doi.org/10.2196/40150.
11. Reitsema M, van Hoek AJ, van der Loeff MS, Hoornenborg E, van Sighem A, Wallinga J, et al. Preexposure prophylaxis for men who have sex with men in the Netherlands: impact on HIV and *Neisseria gonorrhoeae* transmission and cost-effectiveness. AIDS 2020;34(4):621 – 30. https://doi.org/10.1097/QAD.0000000000002469.
12. Celum C, Baeten JM. Lessons on PrEP from the SEARCH study in east Africa. Lancet HIV 2020;7(4):e219 – 20. https://doi.org/10.1016/S2352-3018(20)30003-5.
13. Leech AA, Burgess JF, Sullivan M, Kuohung W, Horný M, Drainoni ML, et al. Cost-effectiveness of preexposure prophylaxis for HIV prevention for conception in the United States. AIDS 2018;32(18): 2787 – 98. https://doi.org/10.1097/QAD.0000000000002014.
14. Jijón S, Molina JM, Costagliola D, Supervie V, Breban R. Can HIV epidemics among MSM be eliminated through participation in preexposure prophylaxis rollouts? AIDS 2021;35(14):2347-54. http://dx.doi.org/10.1097/QAD.0000000000003012.
15. Stover J, Glaubius R, Kassanjee R, Dugdale CM. Updates to the spectrum/AIM model for the UNAIDS 2020 HIV estimates. J Int AIDS Soc 2021;24 Suppl 5(Suppl 5):e25778. http://dx.doi.org/10.1002/jia2.25778.

SUPPLEMENTARY MATERIAL

Structure of the Spectrum Software

Spectrum is a policy module system designed to support the analysis, planning, and advocacy efforts of health programs (*1*). This system, along with its associated manuals, undergoes regular updates and is accessible in various languages at no cost via https://avenirhealth.org/software-spectrum.php. Funding for module development has been primarily provided by the United States Agency for International Development, with additional technical assistance from a group of collaborators including the Joint United Nations Programme on HIV/AIDS, World Health Organization, United Nations Children's Fund, the United Nations Population Division, the United States Census Bureau, United Nations Fund for Population Activities, among others. For this study, we employed four specific modules from the Spectrum suite — namely, the Demographic module (DemProj), the AIDS Impact module (AIM), the Resource Needs module [Chinese yuan (CNY)], and the Goals module — to assess the cost-effectiveness of comprehensive HIV interventions in six eastern Chinese cities. The DemProj module was used to project age- and sex-specific population totals for each city, drawing on fertility and mortality assumptions. The AIM module provided projections of the HIV epidemic's impact, such as the number of people living with HIV, new infections, and age- and sex-specific AIDS mortality. The RNM supplied estimates of the resources required for various interventions, based on coverage data and unit costs previously ascertained in the six cities (*2*). Finally, the Goals module calculated the costs, infections averted, and deaths prevented as a result of the HIV interventions.

Data Collection

Utilizing the Spectrum framework, our team designed a methodical and scalable data collection instrument from the perspective of healthcare payers to streamline the process of calculating costs and constructing models. We consolidated a comprehensive array of indicators, organizing them into a practical instrument comprising 6 primary and 66 secondary categories (*2*). The primary indicators encompass demographic statistics, numbers of HIV-positive individuals and those at elevated risk, strategies for preventing mother-to-child transmission (PMTCT), ART, the scope and expenditure per unit of integrated services, and program logistical support. Meanwhile, the secondary indicators offer detailed quantification of these domains. Experts from the national, provincial, and municipal levels with backgrounds in HIV prevention, treatment, maternal and child healthcare, procurement, and finance were solicited to refine this data collection instrument. A preliminary trial for HIV cost estimation was conducted in Shijiazhuang (*3*). Subsequent data collection in six cities from 2015 to 2019 provided public and service information. Our findings for the comprehensive costs of HIV intervention not only aligned with the realities of the respective locales but also garnered validation from the local expert community.

The CDC in six cities collected data on population size, coverage, unit costs of high-risk populations, and program costs from local demographic, sentinel monitoring, and survey data sources. Data on PMTCT were provided by maternal and child care institutions, while designated hospitals for HIV/AIDS treatment contributed treatment data from hospital information systems. Due to the nature of the study design, personal consent was not deemed necessary. The study received approval from the Ethical Review Committee on Research at the National CDC HIV/STD Center (ID number: X180315504).

Setting Information

To address the lack of regional data, default national-level data for China were utilized in the model, covering aspects like age distribution of fertility, oral PrEP adherence (50%), and PrEP effectiveness (90%). Population mobility was not considered, and the total net migrants per year for each city were set to 0.

After entering all the data into Spectrum, we fitted the model to the epidemic following the software manual.

RESULT

Sensitivity Analysis

Supplementary Table S7 presents remarkable cost-effectiveness results for Shijiazhuang and Ningbo based on selected interventions. The ranking of cost-effectiveness by interventions remained consistent, indicating the

SUPPLEMENTARY TABLE S1. Definitions of all intervention coverage in our study.

Categories	Interventions	Coverage definitions
Selected interventions	VCT	The percentage of the population aged 15–49 years old that receives VCT each year.
	Condoms for adult population	The percentage of the condoms free of charge provided for the population aged 15–49 years old by health institutions each year.
	SSTT	The percentage of secondary school students who have teachers trained in HIV/AIDS education each year.
	FSW outreach	The percentage of female sex workers that is reached by outreach interventions each year.
	MSM outreach	The percentage of MSM that is reached by outreach interventions each year.
	MSM receiving lubricants	The percent of MSM receiving lubricants each year.
	oral PrEP for HRH	The percentage of oral PrEP provided by the health institutions for high-risk heterosexual population each year.
	oral PrEP for MSM	The percentage of oral PrEP provided by the health institutions for MSM each year.
	ART for males	The percentage of males aged 15 years old and above receiving ART to people living with HIV (modeled by Spectrum)each year.
	ART for females	The percentage of females aged 15 years old and above receiving ART to people living with HIV (modeled by Spectrum)each year.
Remaining interventions	Community mobilization	The percentage of the population aged 15–49 years old that is reached by community mobilization efforts each year.
	Mass media	The percentage of the population aged 15–49 years old that is reached by mass media campaigns each year.
	Primary school students with teachers trained in AIDS	The percentage of primary school students who have teachers trained in HIV/AIDS education each year.
	Out-of-school youth reached	The percentage of youth not attending school reached by an HIV/AIDS intervention.
	Cash transfers	The percentage of young women and girls aged 15–24 receiving cash transfers each year.
	Male Sex workers outreach	The percentage of male sex workers that is reached by outreach interventions each year.
	IDUs receiving harm reduction intervention	The percentage of IDUs receiving harm reduction interventions each year.
	IDUs receiving counseling and testing	The percentage of IDUs receiving counseling and testing each year.
	IDUs receiving community outreach and peer education	The percentage of IDUs receiving community outreach or peer education each year.
	IDUs receiving needle and syringe exchange	The percentage of IDUs participating in needle and syringe exchange programs each year.
	IDUs receiving drug substitution	The percentage of IDUs participating in drug substitution programs each year.
	Males with STI receiving treatment	The percentage of males with new and symptomatic STIs that receive treatment each year.
	Females with STI receiving treatment	The percentage of females with new and symptomatic STIs that receive treatment each year.
	Units of blood for transfusion tested	The percentage of blood units tested for HIV each year.
	PEP	The percentage of PEP kits needed that are supplied each year.
	Unsafe injections replaced with AD syringes	The percentage of unsafe injections that are replaced with AD syringes each year.
	Reduction in the number of other injections	The percentage reduction in the number of injections that are not replaced with AD syringes.
	Universal precautions	The percentage of hospital beds that are supplied with universal precautions each year.
	Male circumcision	The percentage of adult males that are currently circumcised in a particular year.

Note: Considering the potential underreporting of HIV infections locally, which could lead to an overestimation of ART coverage rates, we have implemented a consistent approach. ART coverage for both males and females was determined by dividing the reported number of individuals on ART from 2015 to 2019 by the annual estimates of people living with HIV derived from Spectrum using local incidence rates from 2015 to 2019.

Abbreviation: VCT=Voluntary counseling and testing for adult population; SSTT=Secondary students with teachers trained in AIDS; FSW=Female sex worker; MSM=Men who have sex with men; PrEP=Pre-exposure prophylaxis; HRH=High risk heterosexual; ART=Antiretroviral therapy; IDU=Injecting drug user; STI=Sexually transmitted infection; PEP=Post-exposure prophylaxis; AD=Auto-destruct.

robustness of the cost-effectiveness assessment even with variations in unit costs. Comparable patterns were observed in the remaining four cities, although not displayed.

SUPPLEMENTARY TABLE S2. Coverage assumptions for 10 selected HIV interventions in the target year (2028).

Categories	Foshan			Ningbo			Shijiazhuang			Wuxi			Yantai			Zhenjiang		
	Base Scenario	Achievable Scenario	Idealized Scenario	Base Scenario	Achievable Scenario	Idealized Scenario	Base Scenario	Achievable Scenario	Idealized Scenario	Base Scenario	Achievable Scenario	Idealized Scenario	Base Scenario	Achievable Scenario	Idealized Scenario	Base Scenario	Achievable Scenario	Idealized Scenario
	2028	**2028**	**2028**	**2028**	**2028**	**2028**	**2028**	**2028**	**2028**	**2028**	**2028**	**2028**	**2028**	**2028**	**2028**	**2028**	**2028**	**2028**
VCT	0.22	0.44	99.90	0.31	0.62	99.90	0.40	0.80	99.90	0.14	0.28	99.90	0.41	0.82	99.90	0.49	0.98	99.90
Condoms for adult population	0	5.00	99.90	25.41	50.82	99.90	18.75	37.51	99.90	39.09	78.18	99.90	20.48	40.96	99.90	0	5.00	99.90
SSTT	99.90	99.90	99.90	95.00	99.90	99.90	2.50	5.00	99.90	3.00	6.00	99.90	0	5.00	99.90	1.40	2.80	99.90
Female sex workers outreach	99.90	99.90	99.90	72.00	99.90	99.90	28.34	56.68	99.90	99.90	99.90	99.90	92.00	99.90	99.90	94.00	99.90	99.90
MSM outreach	79.32	99.90	99.90	59.20	99.90	99.90	70.00	99.90	99.90	29.94	59.89	99.90	92.70	99.90	99.90	4.80	9.60	99.90
MSM receiving lubricants	79.32	99.90	99.90	0	5.00	99.90	11.21	22.42	99.90	9.98	19.96	99.90	7.20	14.40	99.90	3.90	7.80	99.90
oral PrEP for MSM	0	5.00	99.90	0	5.00	99.90	0	5.00	99.90	0	5.00	99.90	0	5.00	99.90	0	5.00	99.90
oral PrEP for HRH	0	5.00	99.90	0	5.00	99.90	0	5.00	99.90	0	5.00	99.90	0	5.00	99.90	0	5.00	99.90
ART for males	99.90	99.90	99.90	99.90	99.90	99.90	50.86	99.90	99.90	86.14	99.90	99.90	38.61	77.21	99.90	79.48	99.90	99.90
ART for females	99.90	99.90	99.90	99.90	99.90	99.90	16.93	33.86	99.90	42.58	85.16	99.90	10.75	21.50	99.90	49.90	99.79	99.90

Abbreviation: VCT=Voluntary counseling and testing for adult population; SSTT=Secondary students with teachers trained in AIDS; FSW=Female sex worker; MSM=Men who have sex with men; PrEP=Pre-exposure prophylaxis; HRH=High risk heterosexual; ART=Antiretroviral therapy.

SUPPLEMENTARY TABLE S3. Unit cost of 10 selected HIV interventions in six cities (CNY).

Selected HIV interventions	Foshan	Ningbo	Shijiazhuang	Wuxi	Yantai	Zhenjiang	Sources
VCT (costs per test per year)	91.75	326.00	65.00	200.00	389.00	403.21	CDC
Condoms for adult population (costs per condom)	4.50	0.30	2.60	1.64*	0.58	0.20	
SSTT	92.39*	60.00	70.00	92.39*	92.39*	147.16	
FSW reached by intervention per year	50.00	100.00	20.26	100.00	13.90	4.00	
MSM reached by intervention per year	100.00	100.00	122.61*	168.00	122.61*	122.45	
MSM receiving lubricants	5.00	7.75*	2.76	10.00	1.00	20.00	
oral PrEP (costs per person per year)	1,980.00	1,980.00	1,980.00	1,980.00	1,980.00	1,980.00	
ART							Designated hospitals for HIV/AIDS treatment
Adults (costs per patient per year)							
First-line ART drugs	1,134.34*	936.23	1,832.00	715.40	1,136.86	1,051.20	
Second-line ART drugs	4,163.78*	4,343.50	3,577.00	4,526.00	3,846.42	4,526.00	
Additional ART drug costs for TB patients (male)	2,019.46*	2,609.75	1,200.00	4,526.00	1,761.55	0	
Additional ART drug costs for TB patients (Female)	2,029.46*	2,609.75	1,250.00	4,526.00	1,761.55*	0	
Lab costs for ART treatment	2,436.40	1,662.20	1,728.00	3,565.00	3,565.00	1,384.85	
Lab costs for drugs to treat infections	20,000.00	1,000.00	15,000.00	19,459.00	1,1368.77*	1,384.85	
Cotrimoxazole prophylaxis	0.28	120.00	100.00	64.00	80.00	0.10	
TB prophylaxis	0	1,000.00	90.00	200.00	0	15.00	
Nutrition supplements in the first six months	0	0	0	0	0	0	
Children (costs per patient per year)							
Children's ARV drugs	0	6,278.00	0	0	2,656.90	0	
Children's ART treatment lab costs	0	1,142.20	0	0	1,350.00	0	
Service delivery costs							
Cost per in-patient day	600.00	1,000.00	950.00	1,183.00	550.00	856.6*	
Cost per out-patient visit	200.00	500.00	350.00	284.00	250.00	316.8*	
Service delivery requirements (per patient per year)							
ART: in-patient days	7.00	5.00	8.83*	13.00	12.00	7.15	
ART: out-patient visit	4.00	3.00	5.00	4.00	6.00	5.88	
OI treatment: in-patient days	21.00	25.19*	22.00	15.00	28.00*	42.77	
OI treatment: out-patient days	12.00	6.00	4.00	6.00	11.00*	5.00	
Migration from first to second line (% per year)	5.00	3.40	3.30	5.00	1.43	1.63	

Abbreviation: VCT=Voluntary counseling and testing for adult population; SSTT=Secondary students with teachers trained in AIDS; FSW=Female sex worker; MSM=Men who have sex with men; PrEP=Pre-exposure prophylaxis; ART=Antiretroviral therapy; TB= Tuberculosis; OI=Opportunistic infections; CNY=Chinese Yuan.

* indicates cases where the unit cost significantly differed or was missing compared to other cities; in such instances, the average value from the other cities was used to fill in the missing data.

SUPPLEMENTARY TABLE S4. Per capita GDP of the six cities in 2019.

City	Population size			Per Capita GDP (Thousand yuan)
	Male	Female	Total	
Foshan	2,260,855	2,394,761	4,655,616	230.93
Ningbo	4,149,439	4,052,550	8,201,989	146.12
Shijiazhuang	5,536,927	5,414,696	10,951,623	53.05
Wuxi	3,404,656	3,169,859	6,574,515	180.28
Yantai	3,611,082	3,510,713	7,121,795	107.47
Zhenjiang	1,621,496	1,574,911	3,196,407	129.12

Note: Per capita GDP is calculated by dividing the GDP of each city in 2019 (from *the National Economic and Social Development Statistical Bulletin*) by the total population reported by each city.

SUPPLEMENTARY TABLE S5. Total HIV deaths averted by 10 selected HIV interventions in the Achievable Scenario and Idealized Scenario in six cities from 2019 to 2028.

Item	Foshan		Ningbo		Shijiazhuang		Wuxi		Yantai		Zhenjiang	
	AS	IS	AS	IS	AS	IS	AS	IS	AS	IS	AS	IS
VCT	0	0	0	0	0	0	0	0	0	2	0	0
Condoms for adult population	0	0	0	0	0	0	0	0	0	2	0	0
SSTT	0†	0†	0	0	0	0	0	0	0	0	0	0
FSW outreach	0†	0†	0	0	0	0	0†	0†	0	0	0	0
MSM outreach	0	0	0	0	0	0	0	0	0	0	0	0
MSM receiving lubricants*	0	0	0	0	0	0	0	0	0	0	0	0
oral PrEP for MSM	0	0	0	0	0	0	0	0	0	0	0	0
oral PrEP for HRH	0	0	0	0	0	0	0	0	0	0	0	0
ART for males	0†	0†	0†	0†	453	453	15	15	432	545	9	9
ART for females	0†	0†	0†	0†	102	331	115	134	40	235	48	48

Abbreviation: VCT=Voluntary counseling and testing for adult population; SSTT=Secondary students with teachers trained in AIDS; FSW=Female sex worker; MSM=Men who have sex with men; PrEP=Pre-exposure prophylaxis; HRH=High risk heterosexual; ART=Antiretroviral therapy; AS=Achievable Scenario; IS=Idealized Scenario.

* indicates that the impact of MSM receiving lubricants was modeled as 0 in six cities;

† indicates that the baseline intervention coverage reported from the city was 99.9% in 2019, with no room for increase. Therefore, the total deaths averted projected by Spectrum in this city were 0.

SUPPLEMENTARY TABLE S6. Sensitivity analysis with adjusted unit costs in six cities from 2019 to 2028.

City	unit cost+50%								unit cost-50%							
	Incremental cost per infection averted (Thousand yuan)		Times compared to the original unit price		Incremental cost per death averted (Thousand yuan)		Times compared to the original unit price		Incremental cost per infection averted (Thousand yuan)		Times compared to the original unit price		Incremental cost per death averted (Thousand yuan)		Times compared to the original unit price	
	AS	IS	AS	IS	AS	IS	AS	IS	AS	IS	AS	IS	AS	IS	AS	IS
Foshan	712.24	2,975.07	1.5	1.5	158,428.05	656,397.30	1.5	1.5	237.45	992.04	0.5	0.5	52,816.42	218,468.41	0.5	0.5
Ningbo	702.66	9,725.11	1.5	1.5	154,778.00	2,139,229.35	1.5	1.5	234.37	3,297.14	0.5	0.5	51,625.34	725,271.79	0.5	0.5
Wuxi	28.93	243.12	1.5	1.5	83.03	796.85	1.5	1.5	9.79	80.99	0.5	0.5	28.10	265.45	0.5	0.5
Shijiazhuang	89.28	1,517.91	1.5	1.5	226.47	4,647.26	1.5	1.5	29.76	505.92	0.5	0.5	75.50	1,548.93	0.5	0.5
Yantai	36.27	704.36	1.5	1.5	47.78	1,470.50	1.5	1.5	12.11	234.66	0.5	0.5	15.95	489.91	0.5	0.5
Zhenjiang	22.97	1,353.74	1.5	1.5	106.62	8,834.89	1.5	1.5	7.61	451.21	0.5	0.5	35.33	2,944.71	0.5	0.5

Abbreviation: AS=Achievable Scenario; IS=Idealized Scenario.

SUPPLEMENTARY TABLE S7. Sensitivity analysis with unit costs adjusted in Shijiazhuang and Ningbo from 2019 to 2028.

	Ningbo								Shijiazhuang							
	unit cost+50%				unit cost-50%				unit cost+50%				unit cost-50%			
	Incremental cost per infection averted (Thousand yuan)		Times compared to the original unit price		Incremental cost per infection averted (Thousand yuan)		Times compared to the original unit price		Incremental cost per infection averted (Thousand yuan)		Times compared to the original unit price		Incremental cost per infection averted (Thousand yuan)		Times compared to the original unit price	
	AS	**IS**	**AS**	**IS**	**AS**	**IS**	**AS**	**IS**	**AS**	**IS**	**AS**	**IS**	**AS**	**IS**	**AS**	**IS**
VCT	90,971.60	93,980.45	1.5	1.5	30,324.68	31,327.65	0.5	0.5	2,545.60	2,633.91	1.5	1.5	849.32	878.81	0.5	0.5
Condoms for adult population	355.20	361.57	1.5	1.5	119.22	121.35	0.5	0.5	398.32	407.96	1.5	1.5	133.56	136.82	0.5	0.5
SSTT	5,952.32	5,952.32	1.5	1.5	1,931.03	1,931.03	0.5	0.5	389.74	405.18	1.5	1.5	116.94	122.26	0.5	0.5
FSW outreach	3,405.85	3,405.85	1.5	1.5	1,136.14	1,136.14	0.5	0.5	54.32	55.59	1.5	1.5	18.96	19.39	0.5	0.5
MSM outreach	63.71	63.71	1.5	1.5	21.25	21.25	0.5	0.5	0.55	0.55	1.4	1.4	0.23	0.23	0.6	0.6
MSM receiving lubricants	–	–	–	–	–	–	–	–	–	–	–	–	–	–	–	–
oral PrEP for MSM	272.97	292.05	1.5	1.5	91.01	97.36	0.5	0.5	23.07	26.87	1.5	1.5	7.73	9.00	0.5	0.5
oral PrEP for HRH	172,718.24	171,248.66	1.5	1.5	57,573.59	57,083.72	0.5	0.5	14,221.25	14,258.24	1.5	1.5	4,741.25	4,753.59	0.5	0.5
ART for males	–	–	–	–	–	–	–	–	14.43	14.43	1.5	1.5	5.07	5.07	0.5	0.5
ART for females	–	–	–	–	–	–	–	–	13.91	19.00	1.6	1.5	3.42	5.60	0.4	0.5

Note: "–" indicates that the impact was 0 and cannot be divided.

Abbreviation: VCT=Voluntary counseling and testing for adult population; SSTT=Secondary students with teachers trained in AIDS; FSW=Female sex worker; MSM=Men who have sex with men; PrEP=Pre-exposure prophylaxis; HRH=High risk heterosexual; ART=Antiretroviral therapy; AS=Achievable Scenario; IS=Idealized Scenario.

REFERENCES

1. Stover J, Glaubius R, Teng Y, Kelly S, Brown T, Hallett TB, et al. Modeling the epidemiological impact of the UNAIDS 2025 targets to end AIDS as a public health threat by 2030. PLoS Med 2021;18(10):e1003831. https://doi.org/10.1371/journal.pmed.1003831.
2. Zhang YR, Wang LL, Jiang Z, Yan HJ, Liu XX, Gu JY, et al. Estimating costs of the HIV comprehensive intervention using the spectrum model - China, 2015-2019. China CDC Wkly 2022;4(25):554 – 9. https://doi.org/10.46234/ccdcw2022.119.
3. Jiang Z, Zhang YR, Wang LL, Wu ZY. Exploration on the cost estimation tool for HIV comprehensive health intervention according to spectrum theoretical framework. Chin Health Econ 2021;40(3):61-5. (In Chinese). https://kns.cnki.net/kcms/detail/detail.aspx?dbcode=CJFQ&dbname=CJFQ&filename=WEIJ202103021.

Youth Editorial Board

Indexed by Science Citation Index Expanded (SCIE), Social Sciences Citation Index (SSCI), PubMed Central (PMC), Scopus, Chinese Scientific and Technical Papers and Citations, and Chinese Science Citation Database (CSCD)

The inauguration of *China CDC Weekly* is in part supported by Project for Enhancing International Impact of China STM Journals Category D (PIIJ2-D-04-(2018)) of China Association for Science and Technology (CAST).

CCDC weekly

Vol. 6 No. 20 May 17, 2024

Responsible Authority
National Disease Control and Prevention Administration

Sponsor
Chinese Center for Disease Control and Prevention

Editing and Publishing
China CDC Weekly Editorial Office
No.155 Changbai Road, Changping District, Beijing, China
Tel: 86-10-63150501, 63150701
Email: weekly@chinacdc.cn

CSSN
ISSN 2096-7071
CN 10-1629/R1